Article:
Kew, B orcid.org/0000-0003-4550-6999, Holmes, M orcid.org/0000-0002-6819-1048, Stieger, M orcid.org/0000-0002-8736-6026 et al. (1 more author) (2021) Oral tribology, adsorption and rheology of alternative food proteins. Food Hydrocolloids, 116. 106636. ISSN 0268-005X

https://doi.org/10.1016/j.foodhyd.2021.106636

Oral tribology, adsorption and rheology of alternative food proteins

*Ben Kew[1], Melvin Holmes[1], Markus Stieger[2] and Anwesha Sarkar[1]**

[1]Food Colloids and Bioprocessing Group, School of Food Science and Nutrition, Faculty of Environment, University of Leeds, Leeds, LS2 9JT, UK

[2]Division of Human Nutrition and Health, Wageningen University, PO Box 17, 6700 AA Wageningen, The Netherlands

Corresponding author:

*Prof. Anwesha Sarkar

Food Colloids and Bioprocessing Group,

School of Food Science and Nutrition,

University of Leeds, Leeds LS2 9JT, UK.

E-mail address: A.Sarkar@leeds.ac.uk (A. Sarkar).

Graphical Abstract

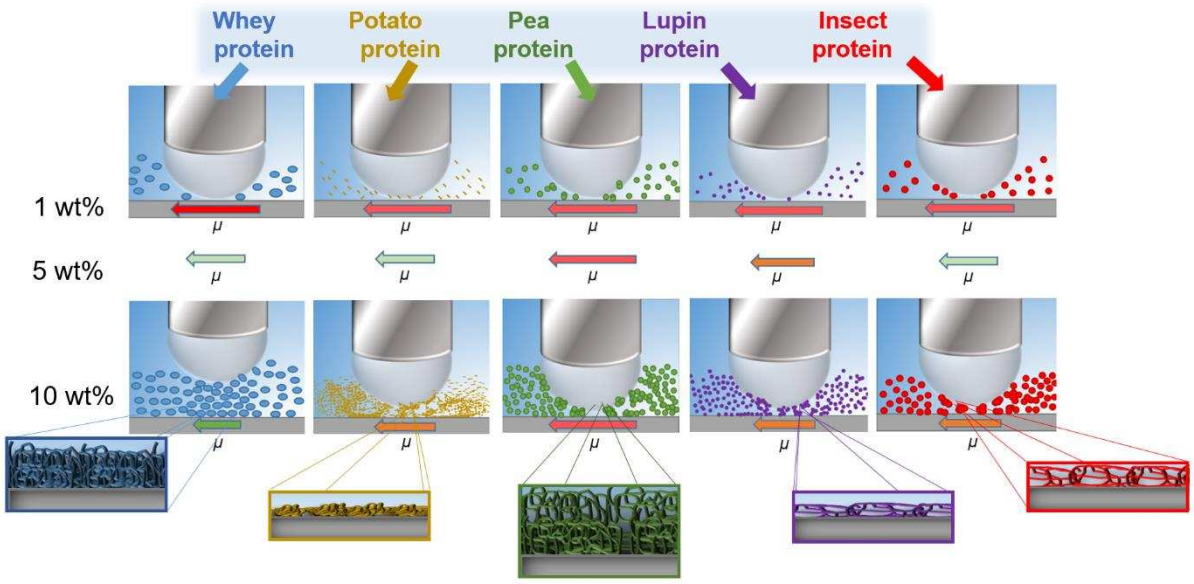

Abstract

Mechanistic knowledge using tribology and adsorption may help to screen various proteins with better lubrication; aiding the fast tracking of new ingredient formulations for use in low-fat/ high protein food development. The aim of this study was to compare the lubrication, adsorption and physicochemical properties of alternative proteins (pea, potato, lupin and insect proteins) with whey protein isolate (WPI) as the control. Soluble fractions (1-10 wt%) of pea protein concentrate (PPC_{sol}), insect protein concentrate (IPC_{sol}), potato protein isolate ($PoPI_{sol}$) and lupin protein isolate (LPI_{sol}) were chosen as the alternative proteins. All proteins were negatively-charged at neutral pH and showed various degrees of aggregation (hydrodynamic diameters ranging from 25 nm for $PoPI_{sol}$ to 244 nm for PPC_{sol}). The boundary friction coefficient (μ) at 5 wt% protein followed the trend as PPC_{sol}> LPI_{sol}> IPC_{sol}> $PoPI_{sol}$> WPI_{sol}, highlighting excellent lubrication performances of $PoPI_{sol}$, IPC_{sol} and WPI_{sol}. At higher protein concentrations (10 wt%), μ significantly increased for LPI_{sol}, $PoPI_{sol}$ and IPC_{sol}, while decreasing for WPI_{sol}. Quartz crystal microbalance with dissipation monitoring (QCM-D) results revealed formation of rigid elastic films on hydrophobic surfaces by $PoPI_{sol}$ and WPI_{sol} giving rise to low μ while more viscous films by PPC_{sol} led to high μ. PPC_{sol} had the highest hydrated mass (11.0 mg m^{-2}) as compared to WPI_{sol} (8.0 mg m^{-2}) with lower values reported for other proteins (5.0-5.4 mg m^{-2}). Strong correlations existed between μ scaled to viscosity, size and hydrated mass and viscoelasticity of films in alternative proteins, validating the surface-linked phenomena in frictional response.

Keywords

Friction; plant protein; QCM-D; viscosity; sustainability; insect protein

1. Introduction

There exists a great possibility for proteins to act as a fat replacer in food formulation; providing less than half the calories of fat (4 kcal per gram), having the highest satiety-providing ability of the macronutrients (Veldhorst, et al., 2008) with some of them having the ability to act functionally as fat mimetic after suitable modifications (Kew, Holmes, Stieger, & Sarkar, 2020). Although there have been several recent studies and industrial developments in this direction using proteins either alone (Nastaj, Terpiłowski, & Sołowiej, 2020), in combination with thickeners (Graf, Protte, Weiss, & Hinrichs, 2020), or in advanced microstructural forms (*e.g.* microparticulated proteins) (Sánchez-Obando, Cabrera-Trujillo, Olivares-Tenorio, & Klotz, 2020), often such fat replacement strategies fail in mimicking the lubricating mouthfeel of fat leading to the rejection of the product by consumers.

Rheological analyses such as viscosity, water holding capacity, compression tests and particle size have typically aided macro-formulation with proteins (Laiho, Williams, Poelman, Appelqvist, & Logan, 2017). However, rheology and particle size do not paint a complete picture on predicting mouthfeel attributes that are lubrication-dominant such as creaminess, smoothness *etc.* (Chen & Stokes, 2012; Kokini, Kadane, & Cussler, 1977; Pradal & Stokes, 2016; Prakash, Tan, & Chen, 2013; Sarkar & Krop, 2019)

Tribology, the study of lubrication and friction has therefore gained much interest recently for its ability to characterise and enhance our understanding of fat-related and more broadly surface-induced mouthfeel perception. A tribometer is utilised to measure such lubrication in which friction coefficients at range of entrainment speeds are measured. Consequently, a distinct Stribeck curve is generated where friction coefficient is plotted against film thickness with identification of three defined lubrication regimes; boundary, mixed and hydrodynamic regime

(Sarkar, Andablo-Reyes, Bryant, Dowson, & Neville, 2019; Stokes, Boehm, & Baier, 2013). It is generally in the boundary and mixed regimes, where friction tends to correlate with a range of friction-related sensory properties *i.e.* smoothness, slipperiness, pastiness, melting *etc.* (Chen & Stokes, 2012; Kokini, Kadane, & Cussler, 1977; Pradal & Stokes, 2016; Prakash, Tan, & Chen, 2013; Sarkar & Krop, 2019). Although biopolymers in general have attracted significant research attention for tribological analysis, systematic tribological characterization of proteins is fairly limited in literature to date (Chojnicka, de Jong, de Kruif, & Visschers, 2008; Kew, Holmes, Stieger, & Sarkar, 2020; Zembyla, et al., 2021).

To advance our fundamental understanding of lubrication in tribological analysis, adsorption techniques such as quartz crystal-microbalance with dissipation (QCM-D) has been utilised recently. Such techniques have been elegantly employed by Stokes, Macakova, Chojnicka-Paszun, de Kruif, and de Jongh (2011) using hydrophobically modified sensors to mimic the surfaces used in tribotesting. Such modification of surfaces in QCM-D offers advanced insights into real-time adsorption of proteins onto hydrophobic surfaces providing information about the viscoelasticity and thickness of the lubricating film indirectly providing information about the frictional phenomena (Glumac, Ritzoulis, & Chen, 2019; Xu, et al., 2020a). Therefore, tribology coupled with QCM-D may provide in-depth fundamental understanding of the adsorbed layers of proteins. Such mechanistic knowledge will not only help to understand lubrication properties of proteins, but may provide an opportunity to screen various proteins with better lubrication properties and help in accelerating the design of new ingredient formulations for use in low-fat/high protein food development.

Whey protein isolate (WPI) has been extensively used in literature for fat replacement owing to its neutral taste and the ability to enhance fatty mouthfeel (Guzmán-González, Morais,

Ramos, & Amigo, 1999; Lesme, et al., 2019) with the ability to reduce friction in tribology by hydration lubrication (Zembyla, et al., 2021) or in the case of microparticulated whey proteins/ microgels, a proposed ball-bearing phenomena (Liu, Tian, Stieger, van der Linden, & van de Velde, 2016b; Sarkar, Kanti, Gulotta, Murray, & Zhang, 2017) . Protein powders, especially WPI are also popular in high protein snacks and drinks consumed after exercise or in body building to promote muscle recovery and hypertrophy (Hulmi, Lockwood, & Stout, 2010). With sustainability now at the forefront of product development requiring lower usage of environmental resources and lower emission, alternative plant- or insect-based proteins are gaining increasing momentum in product development. Alternative proteins although interesting from a sustainability viewpoint often suffer from limited solubility, aggregation, sensorial off taste and unpleasant textural perception, such as sandiness, astringency, dryness *etc.*, which needs attention in literature.

Soy protein has been historically the alternate plant protein of choice (Dabija, Codina, Anca, Sanduleac, & Lacramioara, 2018) because of its ability to increase viscosity and mimic melting properties of fat in various dairy applications (Liu, Wang, Liu, Wu, & Zhang, 2018) and meat replacement (Belloque, García, Torre, & Marina, 2002). Nevertheless, it has often been negatively perceived being an allergen and associated with off-flavours (Damodaran & Arora, 2013). Soy proteins have also shown interesting lubrication ability, with friction coefficients reduced to 0.1 when micro-particulated with further reduction by an order of magnitude when combined with egg white protein (Zhang, et al., 2020b). Besides soy protein, pea protein has recently gained considerable interests in product formulation since it is hypoallergenic. Recent work by Zembyla, et al. (2021) has shown that pea protein has lubrication ability at low concentrations (1-10 mg/mL). However, pea protein tends to aggregate at higher concentrations (>100 mg/ mL) and such transition from dissolved polymer- to aggregated particle-like behaviour

results in lubrication failure. In contrast, whey protein shows increased lubrication at higher concentrations. With the ever expanding research of food proteins, their diversity, application and sourcing, new commercially available proteins are appearing every year. Promising proteins include alternative and tolerably grown legumes like lupin protein and vegetable waste protein like potato protein. With the growing importance of high yield, efficient protein production, but limited by food-neophobia, even insects are being made into protein powders, in all of which, lubrication and adsorption properties have never been investigated, which can help in designing products with optimized mouthfeel.

To summarize, tribological, adsorption and rheological analyses of alternative plant and insect proteins are essential to give a useful reference on how these proteins could be used to replace whey proteins. Hence, the objective of this study was to systematically characterize the lubrication and physiochemical properties of alternative proteins using whey protein as a control, at various protein concentrations. Soluble fractions of vegetable protein (potato protein isolate), legumin-rich proteins (pea protein concentrate, lupin protein isolate) and insect protein concentrate (*Alphitobius diaperinus*) were selected to cover a broad range of sustainable alternative proteins. We characterized their material properties for the first time using tribology, rheology, electrophoresis, dynamic light scattering and adsorption techniques using quartz crystal microbalance with dissipation (QCM-D). Pearson's correlation was employed to correlate frictional data and other measured instrumental parameters. The fundamental insights generated in this work aims to influence future product development with alternative proteins focussing on bulk and surface properties.

2. Materials and Methods

2.1 Materials

Whey protein isolate (WPI) was obtained from Fonterra (Auckland, New Zealand) containing ≥ 96% protein. Pea protein concentrate (PPC, Nutralys S85 XF) containing 85% protein was kindly gifted by Roquette (Lestrem, France). Potato protein isolate (PoPI) was purchased from Guzmán Gastronomía (Barcelona, Spain) containing 91% protein. Insect protein concentrate (IPC, Alphitobius diaperinus) with a protein content of 68% was kindly donated by Protifarm (Ermelo, The Netherlands). Lupin protein isolate (LPI) containing 91% protein was purchased from Prolupin GmbH (Grimmen, Germany). Sodium dodecyl sulphate polyacrylamide gel electrophoresis (SDS-PAGE) reagents including Bolt™ 4–12% Bis-Tris Plus gels, 20× Bolt™ sodium dodecyl sulphate (SDS) running buffer, 4 × Bolt™ lithium dodecyl sulfate (LDS) sample buffer and PageRuler™ Plus Pre-stained protein ladder were purchased from Thermo Fisher Scientific (Loughborough, UK). All solutions were prepared from analytical grade chemicals unless otherwise mentioned. The solvent used was Milli-Q water (purified using Milli-Q apparatus, Millipore Corp., Bedford, MA, USA).

2.2 Preparation of protein samples

Aqueous solutions of the proteins *i.e.* WPI, LPI, PoPI, PPC and IPC (1-10 wt% protein) were prepared by dispersing and mixing the protein powders in 20 mM HEPES (4-(2-hydroxyethyl)-1-piperazineethanesulfonic acid) buffer at pH 7.0 for two hours. These aqueous dispersions were then centrifuged at 20, 000 *g* for 30 minutes and the supernatant was used as the soluble fraction with subscript ‘sol’ for further characterization (see **Table 1** for nomenclature). Due to the low solubility for PPC and inability to mix at high concentrations, the centrifuged supernatant was

extracted, freeze dried and then the soluble PPC powder was used to make protein solution of 10 wt% using 20 mM HEPES buffer at pH 7.0, which was further diluted to 1 or 5 wt%.

2.3 Protein solubility

The solubility of proteins was estimated following Bio-Rad *DC* Protein assay using Coomassie blue at an absorbance of 750 nm. A calibration curve was created using bovine serum albumin (BSA) at 0.2-1.2 mg/mL concentrations and the solubility of each protein was determined as a percentage of protein remaining in supernatant compared to the non-centrifuged initial sample.

2.4 Particle size

Protein solutions were diluted to 0.1 wt% and filtered using a 0.22 μm syringe filter (PTFE Syringe filters, Perkin Elmer, USA) for particle size measurement using dynamic light scattering (DLS) experiments. The mean hydrodynamic diameters (d_H) of the proteins were measured using a Zetasizer Ultra, Malvern Instruments Ltd, Worcestershire, UK. The samples in DTS0012 disposable cuvettes (PMMA, Brand Gmbh, Wertheim, Germany) were introduced in the Zetasizer. The refractive index (RI) of the protein solution was set at 1.45 with an absorption of 0.001. Samples were equilibrated for 120 seconds at 25 ^{o}C and analysed using backscattering technology at a detection angle of 173^{o} in triplicate. The diffusion coefficient (D) was used to obtain d_H considering the dissolved proteins to be spherical using the Stokes-Einstein equation (1):

$$d_H = \frac{k_B T}{3\pi\eta D} \quad (1)$$

where k_B is the Boltzmann constant, T is the temperature, η is the viscosity of the aqueous solution.

2.5 Sodium dodecyl sulphate polyacrylamide gel electrophoresis (SDS-PAGE)

Each protein solutions (32.5 µL) at a concentration of 1 mg/mL were added to 5.0 µL of pre-prepared solution containing 0.078 g of Dithiothreitol (DTT) in 1 mL of Milli-Q and 12.5 µL of Bolt™ LDS sample buffer. The solution was heated at 95 °C for 5 min and 10 µL of the sample + buffer mixture was loaded onto the precast gels placed on an Invitrogen™ Mini Gel Tank system (Thermo Fisher Scientific, Loughborough, UK) submerged in a solution of running buffer: Milli-Q (1:20 v/v). Protein molecular weight marker (5 µL) was added in the first lane of the gels. After running the gel at 200 V for 22 min, the gel was fixed using Milli-Q: Methanol: Acetic acid (5:4:1 v/v) solution for 1 hour and stained for 2 hours with Coomassie Brilliant Blue R-250 solution in 20 vol% isopropanol. The gels were destained overnight in Milli-Q water and scanned using a ChemiDoc™ XRS + System with image LabTM Software (Bio-Rad Laboratories, Richmond, CA, USA). The intensities of the protein bands were quantified using Image Lab Software Version 6.0.

2.6 ζ-potential

The electrophoretic mobilities of the protein samples were measured in the Malvern Zetasizer Ultra, Malvern instruments Ltd, Worcestershire, UK at 25 ^{o}C. Diluted samples (0.01 wt% protein) were prepared and measured in a DTS1070 folded capillary electrophoresis cells. Protein particles moved towards one of the charged electrodes at a certain velocity, and the electrophoretic mobility was then converted into ζ-potential using Henry's equation as shown below:

$$U_E = \frac{2\varepsilon\zeta F(ka)}{3\eta} \quad (2)$$

where, U_E is the electrophoretic mobility, ζ is the zeta-potential, ε is the dielectric constant of the medium, η is the viscosity of HEPES buffer which is equivalent to water and $F(k_a)$ Henry's function using the Smoluchowski approximation is taken as 1.5.

2.7 Apparent viscosity

Flow curves of protein solutions (10 wt% soluble protein) were recorded at 37 ºC using a stress-controlled rheometer (Paar Physica MCR 302, Anton Paar, Austria) equipped with a concentric cylinder geometry (inner diameter of the cup is 24.5 mm and diameter of the bob is 23 nm). The samples were sealed off with a thin layer of silicone oil to prevent evaporation. Shear rates from 1 s^{-1} to 1000 s^{-1} were measured. A minimum of three replicates were measured for each protein sample.

2.8 Tribology

The friction coefficient (μ) was obtained using a tribology-cell attachment to the rheometer *i.e.* a glass ball (R = 7.35 mm) on three polydimethylsiloxane (PDMS) pins (6 mm pin height), latter inclined at 45° to the base. Samples were added in an enclosed chamber with an applied glass ball on top of PDMS plates with samples covering all of the PDMS pins with an evenly distributed 2 N load. The sliding speeds were measured upwards and varied from 0.001 to 1 m s^{-1} whilst the

plates remained stationary generating three-sliding point contact. All measurements were performed at 37 ºC with the μ of the HEPES buffer measured as a control

Normal force is related to the total normal load acting on the plates as described in equation (3). Furthermore, the torque sensed by the glass ball is related to total frictional force (F_F) denoted by equation (4).

$$F_L = \sqrt{2F_N} \tag{3}$$

$$F_F = \frac{\sqrt{2T}}{R} \tag{4}$$

Therefore, μ can be expressed as:

$$\mu = \frac{F_F}{F_N} = \frac{T}{F_N R} \tag{5}$$

The PDMS pins were cleaned using ethanol with subsequent ultra-sonication in detergent solution for 10 minutes. Careful attention was given to signs of surface wear before each experiment, which subsequently followed replacement. A minimum of three replicates were measured for each protein sample.

2.9 Quartz crystal microbalance with dissipation (QCM-D)

For QCM-D experiments, PDMS-coated quartz sensors were prepared by spin-coating silica sensors (QSX-303, Q-Sense, Biolin Scientific, Sweden) with a solution of 0.5 wt% PDMS in toluene at 5000 rpm for 30 s with an acceleration of 2500 rpm/s, before leaving overnight in a vacuum oven at 80^{o}C (for details, see Zembyla et al., 2021). Prior to use, the PDMS-coated crystals were further cleaned by immersing in toluene for 1 minute, then 1 minute in isopropanol and a final immersion in Milli-Q for 5 minutes before being dried using nitrogen gas.

Adsorption of protein on PDMS-coated sensors was measured using quartz crystal microbalance with dissipation monitoring (QCM-D, E4 system, Q-Sense, Biolin Scientific, Sweden) (Xu, et al., 2020a). Protein solutions were made at a concentration of 10 wt% and were equilibrated in buffer at (25^{o}C) before measurement. The flow rate was controlled using peristaltic pump at a rate of 100 µL/ min at 25 ^{o}C. For initial measurements, buffer solution was initially injected to obtain a stable baseline reading and then the prepared protein solutions were injected until equilibrium adsorption *i.e.* no change in frequency (*f*) or dissipation (*D*) was recorded. Finally, the buffer was used once more to remove the non-adsorbed protein. Hydrated mass was calculated from the frequency data using viscoelastic Voigt's model (Voigt, 1889), using "Smartfit Model" by Dfind (Q-Sense, Biolin Scientific, Sweden) software. The 3rd, 5th, 7th and 11th overtones was taken into account for data analysis and only 5th overtone is shown in the results. A minimum of three replicates were measured for each protein sample.

2.10 Statistical analysis

All results are reported as means and standard deviations on at least three repeats. Statistical analysis on the significance between data sets was calculated using analysis of variance (ANOVA)

with Tukey post hoc test. Pearson's correlation (r) were used to assess relationships between hydrodynamic diameter, hydrated mass, ratio of dissipation to frequency ($-\Delta D/\Delta f$) and coefficient of friction scaled at high shear rate viscosity ($U\eta_\infty$) in the boundary (at 0.01 Pa m), mixed (at 0.1 Pa m and 0.3 Pa m) and hydrodynamic regimes (at 1.0 Pa m) at 10 wt% protein. Only alternative proteins were included in the Pearson's correlation analyses. Statistical significance of Pearson's correlation was also conducted using Spearman's rank to obtain the *p-values*. All statistical analyses were done using R version 3.5 (R Core Team, 2018, p. 2012).

3. Results and discussion

3.1 Protein solubility and composition

Plant proteins are well known to encounter solubility problems even though pH can typically be far from pI (Zhang, Holmes, Ettelaie, & Sarkar, 2020a). This insolubility can arise due to complex quaternary structures, processing, a strong tendency to self-aggregate and association with other metabolites such as polyphenols in the natural state (Sarkar & Dickinson, 2020). Hence in this study, we first investigated the solubility of the alternative proteins at pH 7.0 and used the supernatant after centrifugation *i.e.* the soluble-fraction of the protein solutions for further characterization.

As shown in **Table 1**, previous studies have reported similar pI for all protein (pH 4-5) and in our results found protein solubility spanned from 32% to 100%, the lowest soluble fractions being PPC and the highest being WPI and PoPI. Simply by observing the changes in the turbidity of the protein solutions, one can their solubility. Visual images in **Figure 1** reveal that WPI is highly translucent, in other words soluble, this was also true for PoPI, latter has a slight amber hue owing to the presence of brown aromatic compounds (Akyol, Riciputi, Capanoglu, Caboni, &

292 Verardo, 2016). This excellent solubility of PoPI has been reported previously with protein
293 subunits, such as patatins and protease inhibitors showing solubility of > 95% and ~ 85%,
294 respectively (Ralet & Guéguen, 2000; Schmidt, et al., 2019). On the other hand, IPC shows
295 somewhat unusual behaviour in that even after centrifugation, the supernatant remained somewhat
296 cloudy but with relatively high solubility of 88%. This turbidity in IPC might have been caused by
297 the scattering of light from some protein aggregates or other particulate contaminants that might
298 be present in the initial protein concentrate. LPI initially demonstrated a cloudy appearance with
299 75% solubility, where the slight yellow colouration was expected due to the carotenoid-induced
300 pigmentation (Wang, Errington, & Yap, 2008).

301 Spray drying is one of the most efficient and cost effective ways to produce protein
302 powders, however, the shear and temperatures employed during the drying process may induce
303 some degree of conformational changes of the protein resulting in reduced solubility. For instance,
304 high homogenization pressures (150 MPa) employed before the drying process have been linked
305 to increased hydrophobicity of LPI resulting in a 75% solubility (Jayasena, Chih, & Abbas, 2011;
306 Sousa, Morgan, Mitchell, Harding, & Hill, 1996). PPC shows the most notable change, from highly
307 cloudy to nearly colourless appearance as a large fraction of insoluble protein was precipitated out
308 upon centrifugation, which confirms the lowest solubility of 32% of the original concentrate
309 (**Figure 1**). Solubility of around 30% has also been observed in a range of pea protein types in
310 previous studies (Chao, Jung, & Aluko, 2018; Lam, Can Karaca, Tyler, & Nickerson, 2018)

311 To understand whether centrifugation removes any particular subunits of proteins, protein
312 composition of the raw samples and the soluble protein fraction *i.e.* supernatant collected after
313 centrifugation was characterized using SDS-PAGE (**Figure 1**, see **Supplementary Figure S1** for
314 the original electrophoresis gels). As expected the centrifugation step did not influence the protein

315 composition of WPI. In both the un-centrifuged and centrifuged fractions, three main bands were
316 visible in the SDS-PAGE of WPI (**Figure 1**) reflecting β-lactoglobulin (β-lg) (18 kDa), which is
317 the most abundant protein typically present at 50-60%, α-lactalbumin (α-la) (14 kDa) at ~15% and
318 bovine serum albumin (BSA) (67 kDa) at ~5-10%. These constituent protein fractions of WPI are
319 extensively evidenced in literature (Adal, et al., 2017; Chihi, Mession, Sok, & Saurel, 2016;
320 Edwards & Jameson, 2014; Kilara & Vaghela, 2004).

321 In case of PoPI, the proteins segmented into three main groups (**Figure 1**). Patatins (~40
322 kDa), which are glycoproteins and act as protein storage, made up just under half the proteins of
323 the PoPI existing naturally as 88 kDa dimers (Ralet, et al., 2000), followed by the lowest molecular
324 weight (MW) bands making up the protease inhibitors (4-25 kDa) and finally enzymes such as
325 lipoxygenases that are present as faint bands. SDS-PAGE reveals the distinctions very well similar
326 to other studies (Schmidt, et al., 2019; Waglay, Achouri, Karboune, Zareifard, & L'Hocine, 2019)
327 with little to no changes in protein after centrifugation, which is concurrent with the solubility data
328 of PoPI (**Figure 1**).

329 In case of PPC, SDS-PAGE reveals the three globulin proteins, vicilin (7S, 32-50 kDa),
330 legumin (11S, 23, 41 kDa) and convicilin (72, 77 kDa) (**Figure 1**), which is in agreement with
331 previous reports (Adal, et al., 2017; Lam, et al., 2018; Oliete Bonastre, 2018). In the PPC
332 supernatant, there was an increase in vicilin and low MW fractions (10-25 kDa) with subsequent
333 loss of ~100 kDa proteins as compared to the un-centrifuged sample. It should be noted the ratio
334 of 11S:7S composition in pea can vary from 0.2-2.0 depending upon the environmental conditions
335 (Lam, et al., 2018) and may present physicochemical differences than need further investigation.

336 LPI displayed multiple bands with centrifugation having a negligible effect on the intensity
337 levels of the bands (**Figure 1**). Lupin proteins are made up of two main groups, the albumins (11-

70 kDa) and the conglutins, latter being the main storage protein for lupin. As seen in the electrogram, conglutins comprised of α-conglutins (11S, 55 kDa) and β-conglutins (7S, 15-80 kDa), which accounts for approximately 33% and 45% of the total protein (Nadal, Canela, Katakis, & O'Sullivan, 2011).

The IPC displayed a rather complex mixture of faint bands in comparison to the other proteins, which might suggest that the protein bands were not effectively separated in the resolving gel (**Figure 1**). There was a small loss in ~10 kDa and ~130 kDa fractions in the supernatant corroborating the solubility data of IPC. The band observed most likely corresponds to the skeletal muscle proteins, which include four main protein fractions, haemolymph (12 kDa), proteinases (24 kDa, 59 kDa), melanization-engaging proteins (85 kDa) and β-glycosidase (59 kDa) (Lacroix, Dávalos Terán, Fogliano, & Wichers, 2019; Yi, et al., 2013). In summary, PPC showed the largest influence of centrifugation on solubility and composition of the proteins followed by IPC with WPI, PoPI and LPI showing negligible influence. Hereafter, only soluble fractions of proteins have been used for characterization of physicochemical properties, tribology and adsorption properties with these soluble fractions of protein being named as WPI_{sol}, PPC_{sol}, $PoPI_{sol}$, IPC_{sol} and LPI_{sol}..

3.2 Physicochemical properties of the soluble protein fractions

Hydrodynamic diameter (d_H) of the protein solutions was measured using DLS. All the proteins showed certain degree of aggregation with d_H ranging from 25 nm to 244 nm, with $PoPI_{sol}$ and PPC_{sol} representing the lowest and highest d_H, respectively (**Table 1**). Often smaller d_H can be associated with higher degree of solubility and lower levels of turbidity. However, this is not that clear with one of the largest (WPI_{sol}) and smallest-sized proteins ($PoPI_{sol}$) both having 100% solubility (**Figure 1**). For WPI_{sol}, the mean d_H was averaged out of three size distribution peaks at

5 nm, 300 nm and a peak in the order of few thousands of nanometres (**Supplementary Figure S2**), which is reflected in its polydispersity index (PDI) (**Table 1**). A high proportion of WPI is *β*-lg, which might correspond to the 5 nm sized peak (Chihi, et al., 2016). Multiple peaks in DLS of WPI have been also observed previously in studies where these distributions have ranged in sizes from 144 to 3000 nm (Nishanthi, Chandrapala, & Vasiljevic, 2017; Sats, et al., 2014) showing high degree of aggregation (Bouaouina, Desrumaux, Loisel, & Legrand, 2006). On the other hand, $PoPI_{sol}$ has the lowest reported d_H (**Table 1**), which may be due to high levels of phenol that promote protein-polyphenol interactions rather than protein-protein aggregation (Ralet, et al., 2000). Also similar to WPI_{sol}, many size distribution peaks ranging from 5 nm to a few hundreds of nanometres are seen in the DLS graph (**Supplementary Figure S2**) for $PoPI_{sol}$, reporting the highest PDI (0.7) among all the proteins studied (**Table 1**).

The d_H of 244 nm was recorded for PPC_{sol} (**Table 1**) with a single peak on the DLS graph shown in **Supplementary Figure S2**, this is in agreement with previous study by Adal, et al. (2017). Small angle X-ray scattering (SAXS) studies have demonstrated that the radius of individual legumin and vicilin are 4.45 and 4.40 nm, respectively. These individual nanometric-sized proteins form the larger secondary aggregate structures as shown in our study (**Table 1**) and is in agreement with previous reports on size obtained using transmission electron micrographs (TEM) (Oliete, Yassine, Cases, & Saurel, 2019) with secondary aggregation ranging from 100-1000 nm. Nevertheless, it is worth noting that in the previous study (Oliete, et al., 2019), PPC was prepared in the lab from flour different to our commercially available PPC, it is likely the processing involving conversion of pea to pea protein powder might have induced different mechanical and thermal processing as compared to our study, increasing protein interaction thus aggregation in the former. Interestingly, PPC_{sol}, LPI_{sol} and IPC_{sol} had single peaks in DLS

(**Supplementary Figure S2**). However, the mean d_H of >100 nm (**Table 1**) in both suggests that there were protein aggregates rather than monomeric proteins, but the protein-protein aggregates in LPI_{sol} and IPC_{sol} were relatively smaller and evenly sized as compared to WPI_{sol}.

All proteins studied had isoelectric points ranging from pH 4.0-5.0 as shown in **Table 1** (Adal, et al., 2017; Bußler, Rumpold, Jander, Rawel, & Schlüter, 2016; Guimarães & Gasparetto, 2005; Jayasena, et al., 2011; Lacroix, et al., 2019; Schmidt, et al., 2019). Therefore, at pH 7.0, it is not surprising that all the proteins studied here displayed negative ζ-potential values ranging from -18.5 to -23.0 mV, and thus the electrostatic repulsion enabled stable protein dispersion in each case as shown in **Figure 1** in the soluble protein fractions.

3.3 Tribology

To understand the tribological behaviour, we measured the friction coefficients of glass-PDMS tribopairs in the presence of proteins at various concentrations (1-10 wt%) to understand the difference between the types of proteins as well as to identify the role of protein concentration dependence on frictional parameters (**Figure 2**).

Figure 2a-d displays that the buffer showed only boundary (U = 0.001 to 0.01 m/s) and mixed regimes (U = 0.01 to 0.3 m/s), which is in line with previous report (Sarkar, Kanti, Gulotta, Murray, & Zhang, 2017). However, the onset of mixed regime was at one order of magnitude lower speed as compared to that of the previous study (U = 0.1 m/s) (Sarkar, et al., 2017). One might expect this discrepancy owing to the hydrophilic-hydrophobic contact (glass-PDMS) used in this study allowing easy entrainment of the buffer to enable the onset of mixed lubrication regime as opposed to being squeezed out of the contact in the case of the hydrophobic-hydrophobic contact (PDMS-PDMS) used in the previous study (Sarkar, et al., 2017).

All the proteins showed a decrease in friction coefficient with an increase in entrainment speed, with protein solutions gradually transferring from the boundary to the mixed lubrication regimes separating the tribopair surfaces. Firstly focusing on low concentration levels (1 wt%) (**Figure 2a**, see **Supplementary Table S1a** for statistical significance), $PoPI_{sol}$, PPC_{sol}, IPC_{sol} show significant decrease in friction compared to the buffer (~ 35% decrease, $p < 0.05$), WPI_{sol} and LPI_{sol}, with the latter proteins showing some decrease but of non-significance compared to the buffer. Upon entering the mixed regime – U_{max} all solutions showed similar friction with no significant differences observed with buffer. Although significant compared to buffer $PoPI_{sol}$, PPC_{sol}, IPC_{sol} friction is high at 0.35-0.40 reflecting little surface separation between glass ball and PDMS contact and insufficient protein for good lubricating properties. It is interesting to note IPC_{sol} at very low entrainment speeds (0.001-0.01 m/s) recorded much lower friction. Although, at this point, it is just a speculation, this behaviour of IPC_{sol} might be associated with some stabilization issue and not necessarily boundary lubrication.

At 5 wt% protein concentration (**Figure 2b**), all proteins exhibited lubrication ability with distinct reduction in friction coefficients irrespective of the lubrication regimes in comparison to the buffer. This is due to a substantial level of protein that is able to form a hydration layer separating the contact surfaces and allowing for increased mobility for the sliding contacts. Interestingly, the most soluble proteins (WPI_{sol}, $PoPI_{sol}$ and IPC_{sol}) showed similar friction coefficient decreases by an order of magnitude in both the boundary ($\mu_{0.01}$) and mixed regimes ($\mu_{0.3}$) as compared to the buffer in equivalent regimes. Both the legumin-rich proteins *i.e.* PPC_{sol} and LPI_{sol} which displayed lower solubility showed similar trend being more lubricating than the buffer but less as compared to WPI_{sol}, $PoPI_{sol}$ and IPC_{sol} ($p < 0.05$) (see **Supplementary Table**

S1b for statistical significance). Solubility may be important for tribology in terms of the ability to bind water and form a lubricating layer upon entrainment.

At the highest concentration used in this study (10 wt%) (**Figure 2c**), protein entrained between contact can be expected to be the maximum, leading to enhancement in lubricity effectiveness, which has been seen in a number of protein-based tribology studies (Liu, Stieger, van der Linden, & van de Velde, 2016a; Zhang, et al., 2020b). In general from most to least lubricating protein followed pattern of WPI_{sol} > $PoPI_{sol}$ > IPC_{sol} > LPI_{sol} > PPC_{sol} ($p < 0.01$). An interesting feature was that WPI_{sol} showed an onset of hydrodynamic regime unlike the alternative proteins (**Figure 2c**). Noteworthy, that WPI_{sol} retained extensive lubrication property at higher concentrations of 10 wt% (**Figure 2c**) with a further decrease in friction coefficients as compared to 5 wt% concentration levels (**Figure 2b)** in complete contrast to the other proteins (see **Supplementary Table S1c** for statistical significance). For instance, $PoPI_{sol}$ had one of the lowest friction coefficients in the boundary regime and showed decrease in boundary friction coefficients by 75% when concentration was raised from 1 to 5 wt% concentration (**Figure 2a-b**), however $PoPI_{sol}$ suffered from a substantial increase of friction coefficient (~50%) when concentration was raised from 5 to 10 wt% (**Figure 2b-c**). Similar percentage decreases and increases in friction coefficients were also observed for $PoPI_{sol}$ in the mixed regime from 1 to 5 wt % (**Figure 2a-b**) and evidently higher when concentration was raised from 5 wt% to 10 wt% (**Figure 2b-c**). The latter behaviour was also found for IPC_{sol}, where the boundary friction coefficient shows a decrease when concentration was raised from 1 to 5 wt% ($\mu_{0.01}$ = 0.34 and 0.10) in **Figures 2a** and **2b**, respectively following an increase of friction at 10 wt% ($\mu_{0.01}$ = 0.15, see **Figure 2c**). LPI_{sol} was also similar in pattern but with only a marginal increase in boundary friction at 10 wt%.

PPC_{sol} at 5 wt% and 10 wt% was the least lubricating protein when compared to all proteins at boundary (0.01 m/s) and mixed regimes (0.1 m/s) and in some speeds even showed overlapping friction to buffer (see **Supplementary Tables S1b** and **S1c** for statistical significance). Even still, at boundary regime a 30% reduction in friction was produced by increasing the concentration from 1 wt% ($\mu_{0.01}$ = 0.33) (**Figure 2a**) to 5 wt% ($\mu_{0.01}$ = 0.23) (**Figure 2b**), with little further reduction in boundary friction when the concentration was raised to 10 wt% ($\mu_{0.01}$ = 0.21) (**Figure 2c**), in line with previous report using different tribopairs (Zembyla, et al., 2021). Similar levels of reduction in PPC_{sol} was also seen for the mixed regime between 1 - 5 wt% ($\mu_{0.1}$ = 0.16 and 0.1) (**Figures 2a** and **2b)** with a slight decrease in 10 wt% concentration ($\mu_{0.1}$ = 0.08) (**Figure 2c**).

In summary (see schematic in **Figure 3**), whey protein shows a concentration dependent lubrication performance with lower concentration of WPI acting as a poor lubricant (1 wt%) and higher concentration (10 wt%) resulting in lower μ. Unlike WPI, until 5 wt% protein concentration, $PoPI_{sol}$ and IPC_{sol} show excellent lubricating properties. However, at higher concentrations (10 wt%), $PoPI_{sol}$ and IPC $_{sol}$ might have undergone protein-protein aggregation in the contact zone. This most likely creates a particle-like behaviour rather than a continuous polymer-like behaviour, which potentially jams the contact region, resulting in limited sliding and thus leads to increased μ unlike WPI_{sol}. This jamming effect is a relatively new phenomenon, which was firstly observed with higher volume fractions of whey protein microgels (Sarkar, et al., 2017) and more recently with pea protein at higher concentration (Zembyla, et al., 2021).

It should also be noted the better lubricating proteins ($PoPI_{sol}$, WPI_{sol}) also displayed DLS particle size peaks in the range of 1 to 10 nm (**Supplementary Figure S2**) as opposed to the aggregated proteins of around a few hundred nanometres for $PPC_{sol,}$ LPI_{sol} and IPC_{sol}, latter again indicating an aggregated *particle-like* rather than *polymer-like* film behaviour saturating the

474 contact zone particularly at higher concentrations. In other words smaller sized proteins may be
475 better entrained, contributing to improved lubrication as seen previously (Liu, et al., 2016a). It
476 should be noted that larger whey protein aggregates have also been reported to enhance lubrication
477 (Chojnicka, et al., 2008) therefore discrepancy in literature as well as a difficulty in measuring
478 hydrodynamic size with accuracy in case of alternative proteins due to aggregation suggest that
479 direct correlation of particle size of protein with tribology might not be straightforward, which is
480 discussed later.

481 Finally, a key aspect of frictional behaviour is the rheological property of lubricant.
482 Particularly, the high shear rate viscosity (η_∞) of the lubricant becomes a highly relevant parameter
483 to understand the frictional behaviour in the mixed and hydrodynamic lubrication regimes
484 (Andablo-Reyes, et al., 2019). It is worth noting that elastohydrodynamic EHL theory (de Vicente,
485 Stokes, & Spikes, 2005) confirms that a very high shear rate is applied in the tribometer and even
486 at very low entrainment speeds, shear rates can be well above 1000 s^{-1}. **Supplementary Figure**
487 **S3** shows the flow curves of all the proteins at 10 wt% concentration level. At shear rates of 1-
488 1000 s^{-1}, the buffer, IPC_{sol}, and LPI_{sol} displayed Newtonian behaviour where viscosity was
489 independent of the shear rate. WPI_{sol}, PPC_{sol} and $PoPI_{sol}$ on the other hand showed shear thinning
490 behaviour, however, they showed plateau region above 10 s^{-1}. The η_∞ at 1000 s^{-1} was used to scale
491 the tribology data (**Figure 2d**) to understand the influence of viscosity on frictional behaviour. It
492 can be seen that alternative proteins, $PoPI_{sol}$, LPI_{sol} and IPC_{sol} overlapped with the buffer in the
493 mixed lubrication regime (0.3 m/s) with PPC_{sol} being significantly higher in friction ($p < 0.05$) and
494 WPI_{sol} significantly lower ($p < 0.05$) (**Supplementary Table S1d**). The boundary lubrication
495 behaviour could not be explained by the viscosity data and indeed adsorption measurement is

crucial to explain those differences in the tribological behaviour, which is discussed in the following section.

3.4 Surface adsorption characteristics

To understand protein-surface interaction and to explain the tribological features particularly in the boundary regime where adsorption can be an important contributing factor, QCM-D was used to measure the adsorbed hydrated mass and the mechanical properties of the protein films. Since PDMS pins were used in tribological experiments, PDMS-coated crystals in QCM-D replicated the hydrophobic character for the adsorption experiments. Buffer was used to obtain a stable baseline reading, and then protein solutions were applied, all of which resulted in substantial decrease in frequency (f) suggesting that proteins were being adsorbed and formed a viscoelastic layer as supported with an increase in dissipation (D) (**Figure 4**). After the proteins had formed a stable layer (*i.e.* no further change in f), the buffer was again used to wash the residual protein that was not effectively adsorbed to the surface. In all the cases, the f increased upon the addition of the subsequent buffer, which suggests that a significant proportion of the proteins were loosely attached to the surface, which were then removed by the washing phase (**Figure 4**).

To understand better the viscoelastic property of the protein films, the ratio of dissipation and frequency *i.e.* $-\Delta D/\Delta f$ is shown in **Figure 5a** and a schematic illustration is shown in **Figure 5b**. This schematic takes into account $-\Delta D/\Delta f$ as well as hydrated mass which is discussed later. A higher $-\Delta D/\Delta f$ indicates a more viscous and less elastic film, one where time to dissipate energy is increased, whilst a lower $-\Delta D/\Delta f$ implies a more rigid quicker dissipating film (Xu, et al., 2020b). For all proteins, the initial layer formed was a viscoelastic one, *i.e.* a loosely packed hydrated film with $-\Delta D/\Delta f$ values ranging from 0.11-0.18 (**Figure 5a**). However, when washed with buffer, the

unabsorbed proteins appeared to be removed with rigidity increasing. Results show that final film viscoelasticity followed the following pattern *i.e.* IPC_{sol}> PPC_{sol}> LPI_{sol} > WPI_{sol}> $PoPI_{sol}$. In other words, $PoPI_{sol}$ and WPI_{sol} formed the most rigid layers as schematically shown in **Figure 5b**, which may be due to the size and mobility of the proteins to pack efficiently. The relative rigidity of $PoPI_{sol}$ as compared to other alternative proteins might be attributed to it small-size (**Table 1**) and large proportion of a single subunit protein that allowed to form a more ordered, compact and rigid hydrated film on the surface (**Figure 5b**). It is also interesting to note that both WPI_{sol} and $PoPI_{sol}$ were the most soluble (**Table 1**) thus hydrated more uniformly as a continuous film, which promoted higher lubrication (**Figure 2b**). Hence, it can be inferred that a rigid continuous layer of hydrated film (**Figure 5**) might be beneficial in reducing boundary friction.

On the other hand, with more complex numbers of subunit proteins (**Figure 1**) and higher aggregation observed in the case of IPC_{sol} and PPC_{sol} (**Table 1**) a rather unordered viscous layer of protein-protein particles adsorbed with trapped water increasing the $-\Delta D/\Delta f$ value (**Figure 5a**). In other words, PPC_{sol} resulted in a film with more viscosity and less rigidity (**Figure 5b**) and thus might have been easily depleted from the boundary region under tribological stress resulting in higher boundary μ (**Figure 2b**).

Figure 6 shows the final hydrated adsorbed mass of the protein. Not surprisingly, PPC_{sol} (11 mg m^{-2}) resulted in significantly higher adsorbed mass as compared to all the remaining proteins, followed by WPI_{sol} (8 mg m^{-2}) with no significant differences being found between $PoPI_{sol}$, LPI_{sol} and IPC_{sol} ($p > 0.05$) representing similar masses of around 5 mg m^{-2}. Reasons as to why PPC_{sol} adsorbs so heavily may be associated with its high degree of aggregation, as discussed previously (Zembyla, et al., 2021).

4. Correlations between various instrumental characteristics

Correlating frictional properties with physical attributes will help to provide mechanistic insights and thus potentially help fast-tracking desirable proteins/ ingredients to act as fat mimetics or replicate the low friction coefficients as found in fats. Therefore, we evaluated the various instrumental data used in this study for alternative proteins with an aim to identify relationships between hydrodynamic diameter, hydrated mass, viscoelasticity ($-\Delta D/\Delta f$) and μ in different regimes scaled to viscosity and the transition point ($U\eta_{min}$) *i.e.* the transition from mixed to hydrodynamic regime where lowest friction coefficient (at μ_{min}) is obtained. Since WPI_{sol} was used as a control in this study and distinctly different in lubrication properties as compared to the alternative proteins, only alternative protein data was used for evaluating the relationships.

Figure 7 shows that μ in boundary ($U\eta_{0.01}$), mixed ($U\eta_{0.3}$) and hydrodynamic lubrication ($U\eta_{1.0}$) regimes are strongly positively correlated (r = 0.96 - 0.99, $p < 0.001$) which is unsurprising as onset friction coefficient in the hydrodynamic regime is related to the mixed regime and in turn likely to be influenced from the reduction in friction in the boundary regime. When observing the relationship between hydrodynamic diameter and μ in all regimes, there is a positive correlation of r = 0.76 - 0.81 (**Figure 7**), with correlation with μ particularly in the boundary regime being highly significant ($p < 0.01$), to our knowledge this is not reported in literature to date. Increased hydrodynamic size of alternative proteins might result in exclusion of the proteins from the contact zone resulting in increased μ in the boundary regime. So, particle sizing can be an interesting starting point to predict boundary lubrication performance.

Hydrated mass determined by QCM-D also positively correlates with μ in all regimes (r = 0.79 – 0.88). In this respect hydrodynamic diameter and hydrated mass also correlate (r = 0.67) and so a larger sized particle with higher hydrated mass may point towards a particle-like

behaviour that induces a physical jamming and friction increasing effect. It should be pointed out that the correlation with μ only in the mixed regime ($U\eta_{\infty 0.3}$) with hydrated mass was significant ($p < 0.05$) and also PoPI $_{sol,}$ LPI $_{sol}$ and IPC $_{sol}$ had non-significant differences in hydrated mass yet different tribological responses. Static measurement of QCM-D adsorption may not accurately portray the film behaviour that is under dynamic conditions during the high shear experienced during tribology, so it might not be straightforward to find a relationship between hydrated mass and μ. Hydrodynamic diameter and $-\Delta D/\Delta f$ are also positively correlated with high significance ($p < 0.001$) suggesting smaller proteins are more likely to form a rigid and packed layer as opposed to larger ones forming a more viscoelastic layer.

A weak positive correlation was found between $-\Delta D/\Delta f$ and lubrication although this is likely due to the large deviations of measurements from IPC $_{sol.}$ We conducted a correlation removing IPC $_{sol}$ focussing just on plant proteins as shown in **Supplementary Figure S4**. With the removal of IPC_{sol}, we observed highly positive correlation (r = 0.9-0.99) with very significance ($p < 0.001$) between $-\Delta D/\Delta f$ values suggesting a rigid layer improves lubrication irrespective of the regimes. This can be explained as the highly viscoelastic layer might be easily removed from the contact region, as opposed to a rigid layer which might remain creating a gap between the contact surfaces reducing μ.

Next when observing $U\eta_{min}$ (at μ_{min}), we can see this is the only parameter producing a negative correlation with all other parameters and further increases in negative correlation in **Supplementary Figure S4** when excluding IPC $_{sol}$. This negative correlation found between the entrainment speed where the friction coefficient is a minimum, corresponding to the transition between the hydrodynamic and mixed regime $U\eta_{min}$ (at μ_{min}), and the wet mass as well as $-\Delta D/\Delta f$ values is in line with the findings previously reported by Stokes, et al. (2011). In other words, we

588 can say that although a rigid layer with lower hydrated mass might be efficient in providing optimal
589 boundary lubrication, presence of a viscoelastic layer might help in accelerating the transition from
590 mixed to boundary lubrication regimes.

591 To sum everything up with respect to correlations for alternative proteins, it can be inferred
592 that proteins with highest lubrication performance investigated within this study have the lowest
593 hydrodynamic diameter, are more rigid and of lower hydrated mass (*i.e.* $PoPI_{sol}$) and the opposite
594 holds true for proteins showing lowest lubrication performance (*i.e.* PPC_{sol}). While statistically
595 speaking, these correlation coefficients appear reasonable, with only four alternative protein types,
596 it is difficult to prove whether such relationships are just empirical or truly causal at this stage.

597 Bartlett tests show that there is significantly correlated data however upon conducting a Kaiser-
598 Meyer-Olkin test the value is less than 0.5 due to the limited number of sample data and ultimately
599 a trend can be predicted but not causative and so these parameters should undergo further
600 investigation. It should be emphasised that more data points would establish stronger evidence and
601 greater confidence in the observed correlations, nonetheless there are clearly strong associations
602 of high statistical significance, which for the first time have been established in such a range of
603 alternative proteins that may serve as a reference to fast track the development of food with
604 optimally lubricating alternative proteins.

605

606 ## 5. Conclusions

607 Lubrication and adsorption properties of alternative proteins sourced from potato, pea, lupin and
608 insects were compared with whey protein. Soluble fractions of these concentrates/isolates were
609 characterised by means of hydrodynamic size, charge, rheology, tribology and adsorption

610 (hydrated mass, film viscoelasticity). The lowest solubility was reported with PPC_{sol}, all other
611 proteins displayed good solubility with complete dissolution being observed for $PoPI_{sol}$ and WPI_{sol}.
612 Proteins were all negatively-charged and showed various degrees of aggregation with
613 hydrodynamic sizes ranging from $PoPI_{sol}$ at tens of nanometres to WPI_{sol} and PPC_{sol} at a couple
614 hundred of nanometres.

615 Strikingly, all alternative proteins showed effective lubrication at 5 wt% concentration
616 following a distinct reduction in friction. PPC_{sol} showed the lowest effective lubrication in
617 comparison to all other proteins with highest friction coefficient amongst the tested proteins at
618 both 5 wt% and 10 wt% concentration. Interestingly, for LPI_{sol} and particularly $PoPI_{sol}$, and IPC_{sol},
619 friction coefficients were increased when concentration was raised from 5 wt% to 10 wt%, most
620 possibly due to aggregation and jamming of the proteins in the contact region behaving like particle
621 aggregates than a lubricating polymeric film. WPI_{sol} was superior in lubrication with lowest
622 boundary friction coefficient even when the concentration was increased to 10 wt%. Results from
623 QCM-D reveal rigid film formation may result in a reduction in boundary lubrication and visa
624 versa for rigid films. Pearson's correlation between alternative protein data plots revealed
625 relationship of lubrication as well as transition between lubrication regimes to hydrated mass,
626 hydrodynamic size and viscoelasticity.

627 It is worth noting that whey proteins showed substantial lubrication performance as
628 compared to alternative proteins particularly at higher concentrations. Nevertheless, alternative
629 proteins may still be utilised to lubricate at lower concentrations. Among the tested proteins, potato
630 protein seems to stand out in its lubrication performance because of its smaller size and ability to
631 form an elastic layer at the surface. Finally, sensory tests are key to understand whether such

increased lubrication, hydrated mass and viscoelasticity are associated with positive mouthfeel perception such as smoothness in alternative proteins.

Acknowledgements

Funding from the European Research Council (ERC) under the European Union's Horizon 2020 research and innovation programme (grant agreement n° 757993) is acknowledged.

Conflict of Interests

Declarations of interest: none

CRediT author statement

Ben Kew: Methodology, Validation, Formal analysis, Investigation, Data curation, Visualization; Project administration; Writing- Original draft preparation, **Melvin Holmes:** Methodology, Validation, Data curation, Writing- Reviewing & Editing; Visualization, Supervision; **Markus Stieger:** Data curation, Visualization; Writing- Reviewing & Editing;; **Anwesha Sarkar:** Conceptualization, Methodology, Writing- Reviewing & Editing, Visualization, Supervision, Funding acquisition

651

652 **Table 1.**

653

Soluble fractions of protein samples	Nomenclature	Isoelectric point (pI)	Solubility	Hydrodynamic diameter (d_H) (nm)	Polydispersity index (PDI)	ζ-potential (mV)
Whey protein isolate	WPI_{sol}	4.5 (Guimarães & Gasparetto, 2005)	100% ± 4.6%^{d}	220.0 ± 30.9^{d}	0.35 ± 0.12^{bc}	-18.5 ± 0.9^{a}
Potato protein isolate	$PoPI_{sol}$	4.5 – 5.0 (Schmidt, et al., 2019)	100% ± 1.0%^{d}	24.7 ± 1.0^{a}	0.7 ± 0.35^{c}	-22.4 ± 1.1^{bc}
Pea protein concentrate	PPC_{sol}	4.0 (Adal, et al., 2017)	32% ± 4.5%^{a}	244 ± 23.6^{d}	0.4 ± 0.005^{bc}	-20.6 ± 1.3^{ab}
Lupin protein isolate	LPI_{sol}	4.5 (Jayasena, et al., 2011)	75% ± 4.0%^{b}	116.0 ± 4.8^{b}	0.3 ± 0.003^{b}	-23.0 ± 0.5^{c}
Insect protein concentrate	IPC_{sol}	4.0 – 4.5 (Bußler, Rumpold, Jander, Rawel, & Schlüter, 2016; Lacroix, et al., 2019)	88% ± 7.8%^{c}	160 ± 3.7^{c}	0.2 ± 0.04^{a}	-20.7 ± 0.9^{b}

654

655

Caption for the Table

Table 1. Physicochemical characteristics of centrifuged and filtered protein solutions at pH 7.0. Error bars indicate standard deviation for triplicate samples (n = 3 × 3 for solubility, $d_{H,}$ PDI and 5 × 3 for ζ-potential). Parameters denoted with the same lower case subscripts do not differ statistically at the confidence of $p \geq 0.05$.

Figure 1.

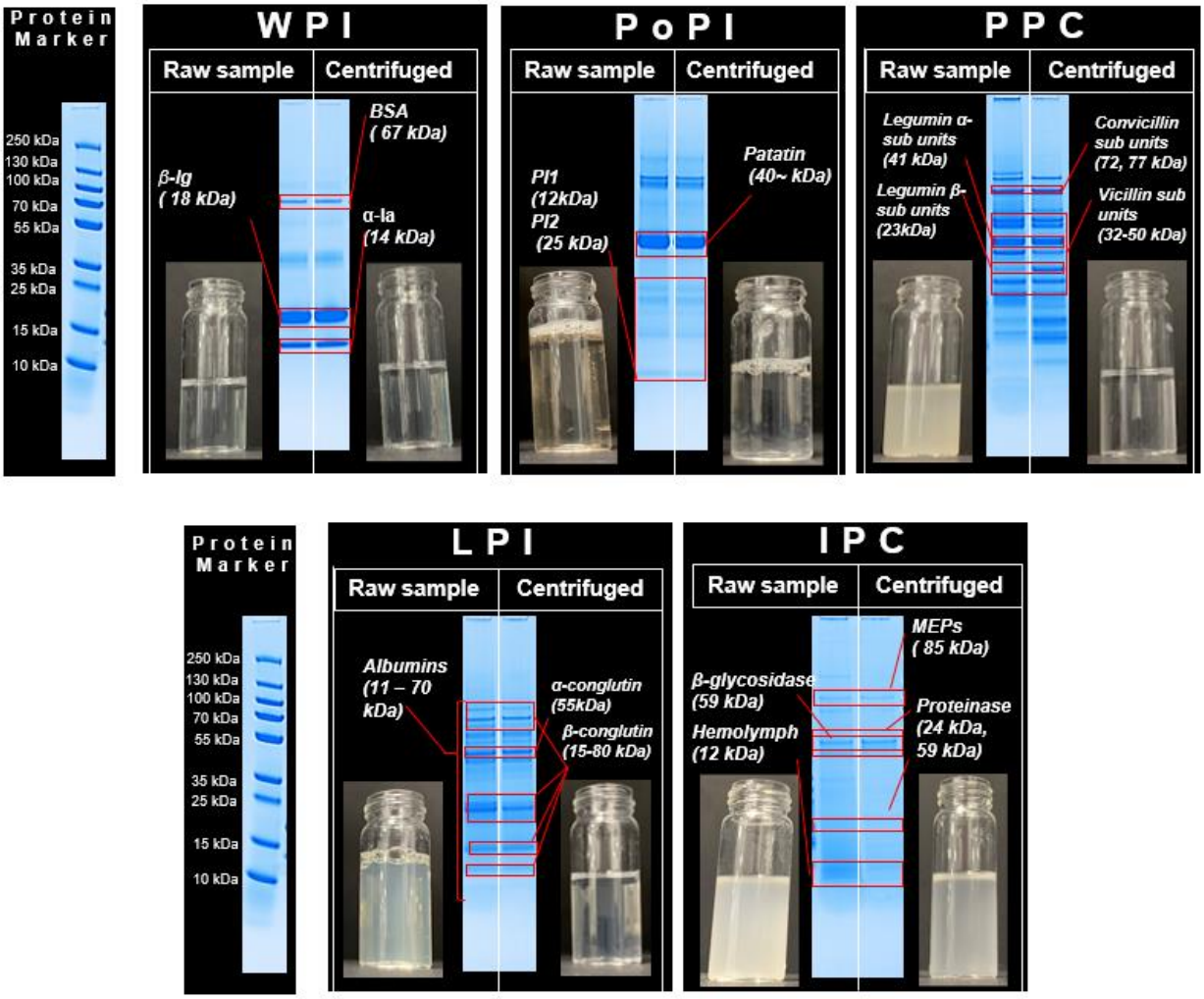
Protein Marker
250 kDa
130 kDa
100 kDa
70 kDa
55 kDa
35 kDa
25 kDa
15 kDa
10 kDa
WPI
Raw sample
Centrifuged
β-lg (18 kDa)
BSA (67 kDa)
α-la (14 kDa)
PoPI
Raw sample
Centrifuged
PI1 (12kDa)
PI2 (25 kDa)
Patatin (40~ kDa)
PPC
Raw sample
Centrifuged
Legumin α-sub units (41 kDa)
Legumin β-sub units (23kDa)
Convicillin sub units (72, 77 kDa)
Vicillin sub units (32-50 kDa)
Protein Marker
250 kDa
130 kDa
100 kDa
70 kDa
55 kDa
35 kDa
25 kDa
15 kDa
10 kDa
LPI
Raw sample
Centrifuged
Albumins (11 – 70 kDa)
α-conglutin (55kDa)
β-conglutin (15-80 kDa)
IPC
Raw sample
Centrifuged
β-glycosidase (59 kDa)
Hemolymph (12 kDa)
MEPs (85 kDa)
Proteinase (24 kDa, 59 kDa)

Figure 2.

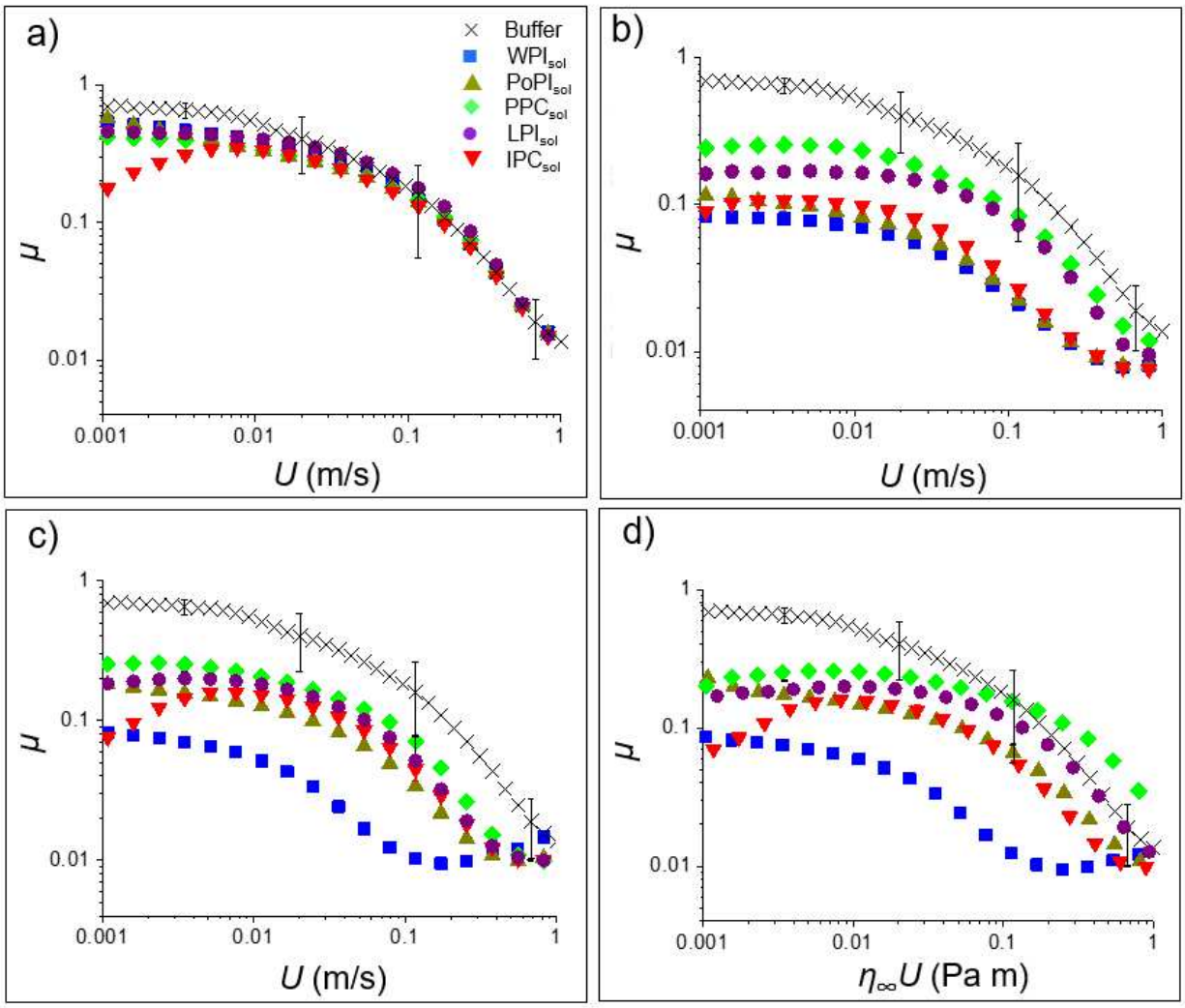
a)
Buffer
WPI$_{sol}$
PoPI$_{sol}$
PPC$_{sol}$
LPI$_{sol}$
IPC$_{sol}$
μ
U (m/s)
b)
μ
U (m/s)
c)
μ
U (m/s)
d)
μ
η∞U (Pa m)

Figure 3.

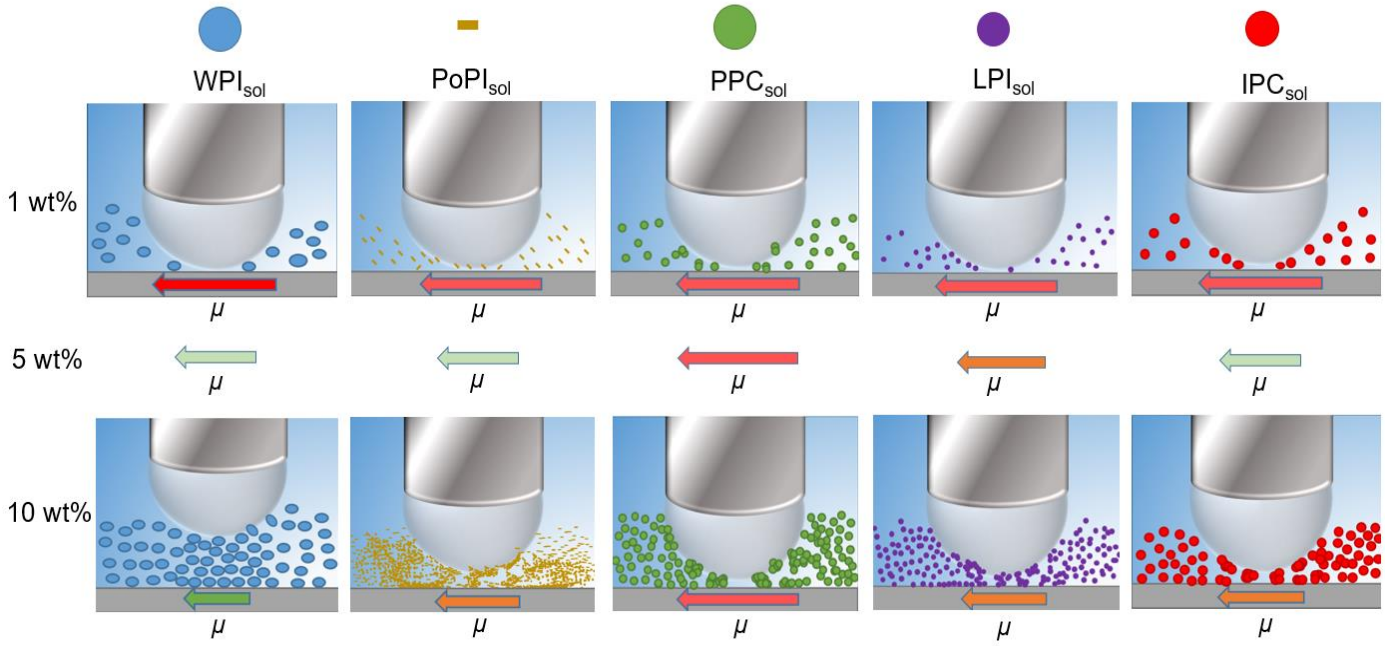

687 **Figure 4.**

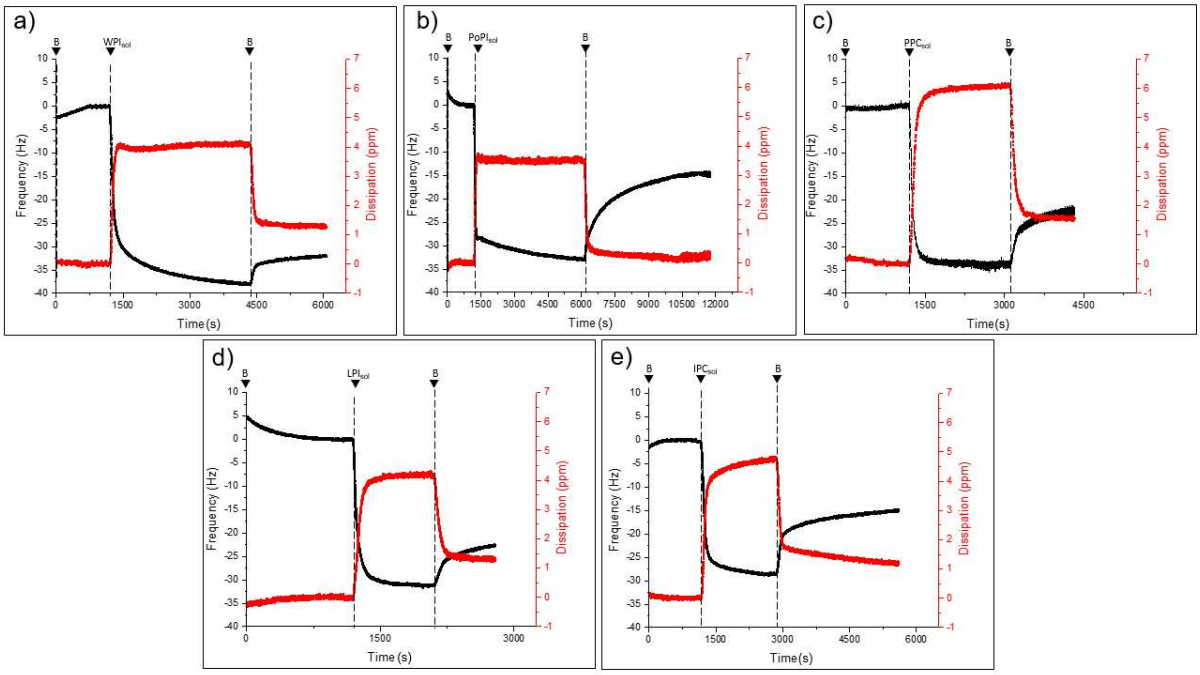

688

689

690

691

692 **Figure 5.**

a)

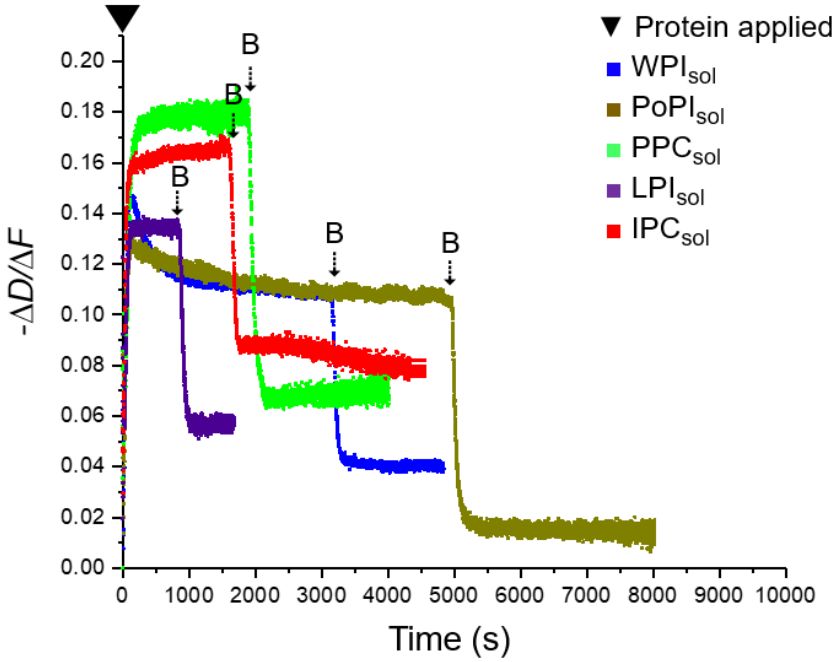

b)

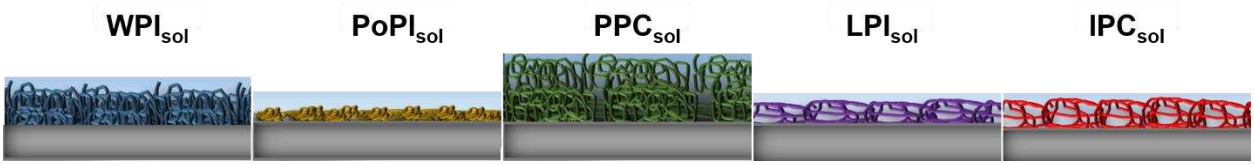

693

694

695

696 **Figure 6.**

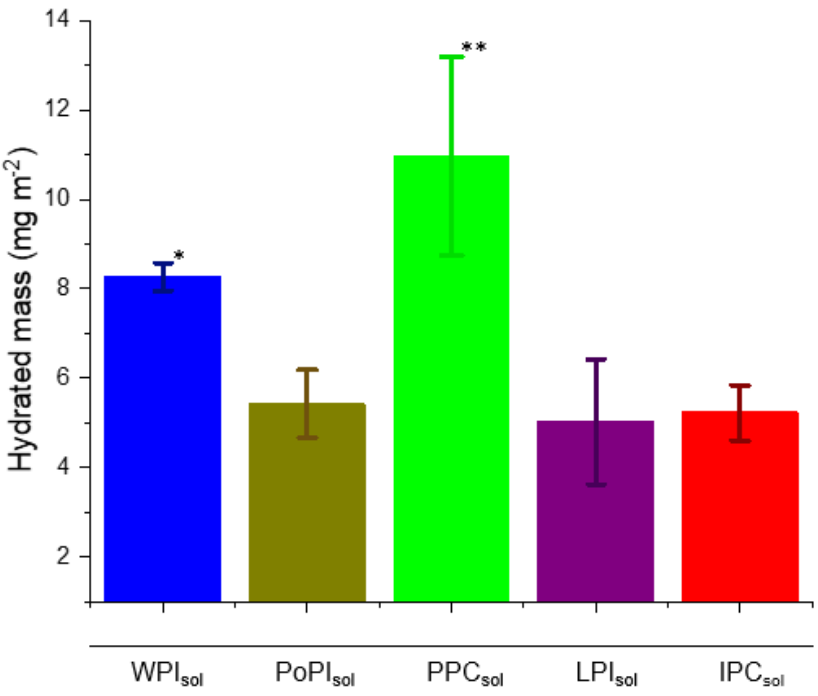

697

698

699

Figure 7.

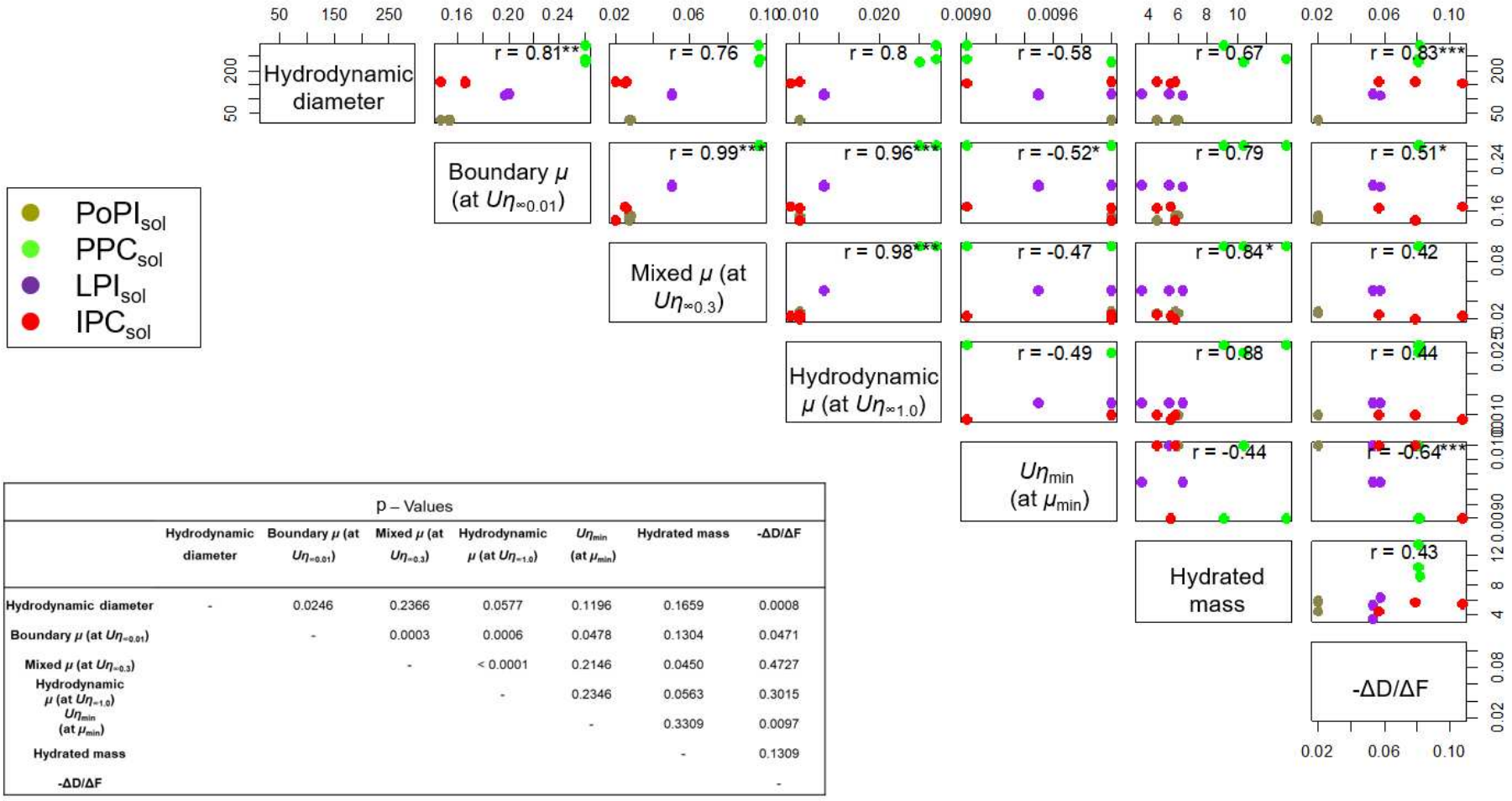

p – Values

	Hydrodynamic diameter	Boundary μ (at $U\eta_{\infty 0.01}$)	Mixed μ (at $U\eta_{\infty 0.3}$)	Hydrodynamic μ (at $U\eta_{\infty 1.0}$)	$U\eta_{min}$ (at μ_{min})	Hydrated mass	-ΔD/ΔF
Hydrodynamic diameter	-	0.0246	0.2366	0.0577	0.1196	0.1659	0.0008
Boundary μ (at $U\eta_{\infty 0.01}$)		-	0.0003	0.0006	0.0478	0.1304	0.0471
Mixed μ (at $U\eta_{\infty 0.3}$)			-	< 0.0001	0.2146	0.0450	0.4727
Hydrodynamic μ (at $U\eta_{\infty 1.0}$)				-	0.2346	0.0563	0.3015
$U\eta_{min}$ (at μ_{min})					-	0.3309	0.0097
Hydrated mass						-	0.1309
-ΔD/ΔF							-

* = p < 0.05 ** = p < 0.01 *** = p < 0.001

Captions for Figures

Figure 1. Sodium dodecyl sulphate polyacrylamide gel electrophoresis (SDS-PAGE) of protein solutions and their % solubility at pH 7.0. Protein fractions are as follows, beta-lactoglobulin (β-lg), bovine serum albumin (BSA), alpha-lactalbumin (α-la), protease inhibitor 1 and 2 (PI1, PI2), melanisation engaging proteins (MEPs).

Figure 2. Mean friction coefficients (μ) as a function of entrainment speed (U) determined between glass ball and PDMS surface at 2 N load in presence of protein solutions at 1.0 wt% (a), 5.0 wt% (b), and 10 wt% (c) protein, respectively and scaling of friction curves (d) of 10 wt% proteins to high shear rate viscosity (η_∞). Friction curves of HEPES buffer are shown in all the graphs. Error bars indicate standard deviation for triplicate experiments (n = 3 × 3).

Figure 3. Schematic representation (not to scale) of the lubrication behaviour of WPI_{sol} $PoPI_{sol}$ PPC_{sol} LPI_{sol} and IPC_{sol} on glass ball on PDMS surface illustrating the effect of concentration and protein type on friction coefficient (μ) (depicted as green, orange and red friction arrows showing lowest friction to highest friction induced by proteins, respectively).

Figure 4. Mean frequency and dissipation (5^{th} overtone shown) of 1.0 wt% WPI_{sol} (a), $PoPI_{sol}$ (b), PPC_{sol} (c), LPI_{sol} (d) and IPC_{sol} (e) on PDMS-coated sensors, respectively and B implies the HEPES buffer.

Figure 5. Dissipation shift (ΔD) / frequency shift (Δf) ratio *i.e.* $-\Delta D/\Delta f$ (a) of 1.0 wt% WPI_{sol}, $PoPI_{sol}$, PPI_{sol}, LPI_{sol} and IPI_{sol} on PDMS-coated hydrophobic sensors. Step B represents the

final buffer rinsing stage to understand the final characteristics of the film. Schematic representation (b) of the hydrated layer of protein films on PDMS surface.

Figure 6. Hydrated mass of protein solutions at pH 7.0 (1.0% w/v) on PDMS-coated hydrophobic sensors using QCM-D. Error bars indicate standard deviation for triplicate experiments (n = 3 × 3). The asterisk represents significant difference ($p < 0.05$)

Figure 7. Pearson correlation (r) of instrumental data for 10 wt% protein solutions where n = 3 for each protein data sets. $-\Delta D/\Delta F$ is the dissipation shift (ΔD) / frequency shift (Δf) ratio. Spearman's rank was used to obtain the *p-values* as an inset table and translated into *, **, *** indicating 0.05-0.001 in order of significance.

Supplementary Document

Oral tribology, adsorption and rheology of alternative food proteins

*Ben Kew[1], Melvin Holmes[1], Markus Stieger[2] and Anwesha Sarkar[1]**

[1]Food Colloids and Bioprocessing Group, School of Food Science and Nutrition, Faculty of Environment, University of Leeds, Leeds, LS2 9JT, UK

[2]Division of Human Nutrition and Health, Wageningen University, PO Box 17, 6700 AA Wageningen, The Netherlands

Corresponding author:

*Prof. Anwesha Sarkar

Food Colloids and Bioprocessing Group,

School of Food Science and Nutrition,

University of Leeds, Leeds LS2 9JT, UK.

E-mail address: A.Sarkar@leeds.ac.uk (A. Sarkar).

Supplementary Table S1. Mean and standard deviation (SD) of the friction coefficients of buffer and soluble protein solutions at 1 wt% (a), 5 wt% (b), 10 wt% (c) and 10 wt% scaled with viscosity at 1000 s^{-1} (η_∞ U (Pa m)) (d). Parameters denoted with the same lower case subscripts do not differ statistically at the confidence of $p \geq 0.05$.

(a)	Coefficient of friction of 1 wt% $protein_{sol}$							
	Boundary lubrication regime (0.01 m s^{-1})		Mixed lubrication regime (0.1 m s^{-1})		Mixed lubrication regime (0.3 m s^{-1})		Hydrodynamic lubrication regime (1.0 m s^{-1})	
	Mean	SD	Mean	SD	Mean	SD	Mean	SD
Buffer	0.509^{c}	0.128	0.182^{d}	0.116	0.056^{abc}	0.035	0.014^{a}	0.005
WPI_{sol}	0.387^{bc}	0.018	0.164^{abd}	0.018	0.051^{ab}	0.007	0.015^{a}	0.001
$PoPI_{sol}$	0.327^{a}	0.005	0.157^{ad}	0.005	0.056^{ab}	0.003	0.013^{a}	0.001
PPC_{sol}	0.332^{a}	0.010	0.164^{bd}	0.001	0.058^{b}	0.001	0.013^{a}	0.001
LPI_{sol}	0.401^{bc}	0.011	0.202^{cd}	0.003	0.066^{c}	0.002	0.013^{a}	0.001
IPC_{sol}	0.335^{a}	0.008	0.149^{ad}	0.005	0.053^{a}	0.002	0.013^{a}	0.001

(b)	Coefficient of friction of 5 wt% $protein_{sol}$							
	Boundary lubrication regime (0.01 m s^{-1})		Mixed lubrication regime (0.1 m s^{-1})		Mixed lubrication regime (0.3 m s^{-1})		Hydrodynamic lubrication regime (1.0 m s^{-1})	
	Mean	SD	Mean	SD	Mean	SD	Mean	SD
Buffer	0.509^{f}	0.128	0.182^{e}	0.116	0.056^{d}	0.035	0.014^{c}	0.005
WPI_{sol}	0.069^{a}	0.005	0.024^{a}	0.002	0.010^{a}	0.001	0.008^{ac}	0.001
$PoPI_{sol}$	0.082^{b}	0.006	0.027^{a}	0.001	0.010^{a}	0.001	0.009^{abc}	0.001
PPC_{sol}	0.234^{e}	0.006	0.097^{de}	0.003	0.031^{cd}	0.002	0.011^{bc}	0.001
LPI_{sol}	0.164^{d}	0.006	0.073^{ce}	0.001	0.024^{bd}	0.001	0.009^{abc}	0.001
IPC_{sol}	0.098^{c}	0.003	0.032^{b}	0.001	0.010^{a}	0.001	0.008^{ac}	0.001

(c)	Coefficient of friction of 10 wt% $protein_{sol}$							
	Boundary lubrication regime (0.01 m s^{-1})		Mixed lubrication regime (0.1 m s^{-1})		Mixed lubrication regime (0.3 m s^{-1})		Hydrodynamic lubrication regime (1.0 m s^{-1})	
	Mean	SD	Mean	SD	Mean	SD	Mean	SD
Buffer	0.509^{f}	0.128	0.182^{f}	0.116	0.056^{d}	0.035	0.014^{b}	0.005
WPI_{sol}	0.051^{a}	0.001	0.011^{a}	0.001	0.010^{a}	0.001	0.016^{bc}	0.002
$PoPI_{sol}$	0.126^{b}	0.002	0.041^{b}	0.001	0.012^{a}	0.001	0.011^{ab}	0.001
PPC_{sol}	0.205^{e}	0.001	0.083^{ef}	0.001	0.020^{cd}	0.001	0.009^{ab}	0.001
LPI_{sol}	0.182^{d}	0.004	0.060^{d}	0.002	0.015^{b}	0.001	0.011^{ab}	0.002
IPC_{sol}	0.152^{c}	0.012	0.054^{c}	0.001	0.015^{b}	0.002	0.010^{ab}	0.001

(d)	Coefficient of friction of 10 wt% $protein_{sol}$ scaled η_∞ U (Pa m)							
	Boundary lubrication regime (0.01 m s^{-1})		Mixed lubrication regime (0.1 m s^{-1})		Mixed lubrication regime (0.3 m s^{-1})		Hydrodynamic lubrication regime (1.0 m s^{-1})	
	Mean	SD	Mean	SD	Mean	SD	Mean	SD
Buffer	0.509^{f}	0.128	0.182^{e}	0.116	0.056^{d}	0.035	0.014^{d}	0.005
WPI_{sol}	0.059^{a}	0.006	0.014^{a}	0.002	0.009^{a}	0.001	0.013^{bcd}	0.002
$PoPI_{sol}$	0.150^{b}	0.004	0.066^{b}	0.001	0.027^{bd}	0.001	0.010^{abd}	0.001
PPC_{sol}	0.260^{d}	0.001	0.163^{de}	0.006	0.096^{e}	0.001	0.026^{e}	0.001
LPI_{sol}	0.199^{c}	0.002	0.125^{ce}	0.003	0.050^{cd}	0.001	0.013^{cd}	0.001
IPC_{sol}	0.159^{b}	0.011	0.064^{b}	0.001	0.023^{bd}	0.003	0.009^{ad}	0.001

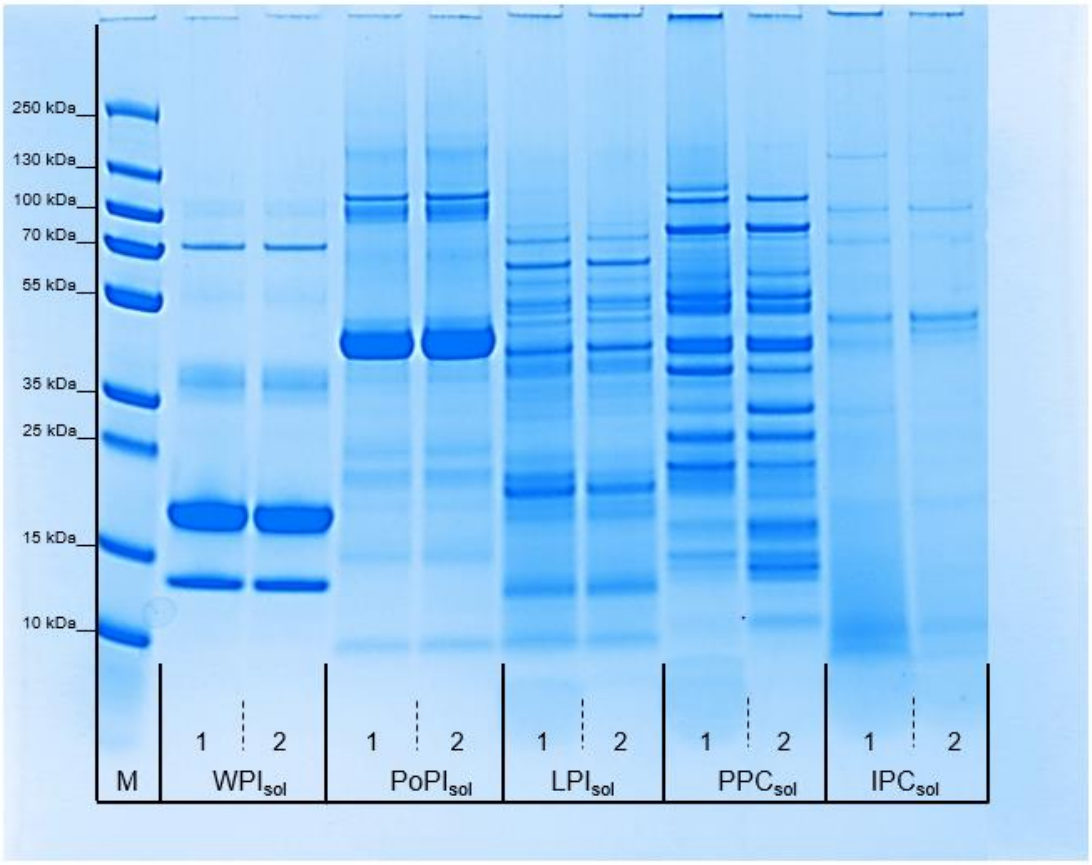

770

771

772 **Supplementary Figure S1**. Raw data of the sodium dodecyl sulphate polyacrylamide gel
773 electrophoresis (SDS-PAGE) of protein solutions at pH 7.0. 1 and 2 refers to the uncentrifuged
774 and centrifuged samples, respectively. M represents the protein marker.

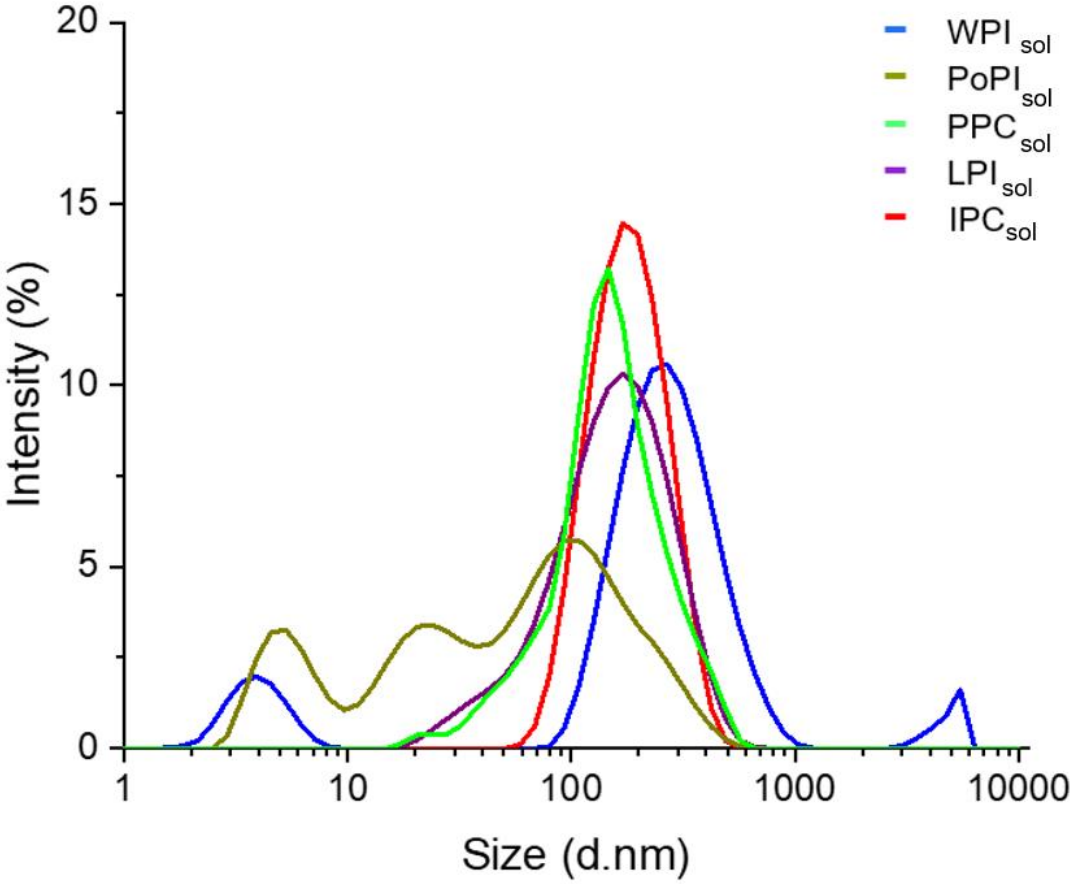

775

776 **Supplementary Figure S2.** Mean particle size distribution of protein samples (0.1 wt%
777 protein) at pH 7.0 after centrifugation and filtration using 0.22 μm syringe filter (n = 3 × 3).

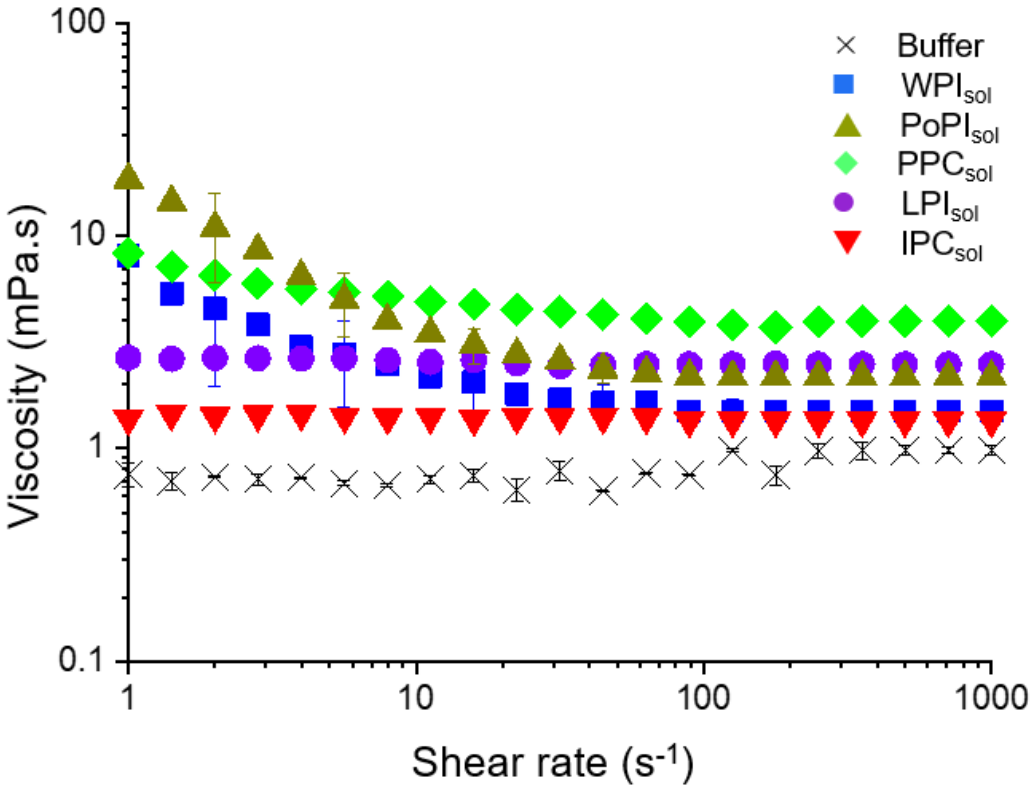

778

779 **Supplementary Figure S3.** Flow curves of protein solutions (10 wt% protein) at pH 7.0.
780 Error bars indicate standard deviation for triplicate experiments (n = 3 × 3).
781

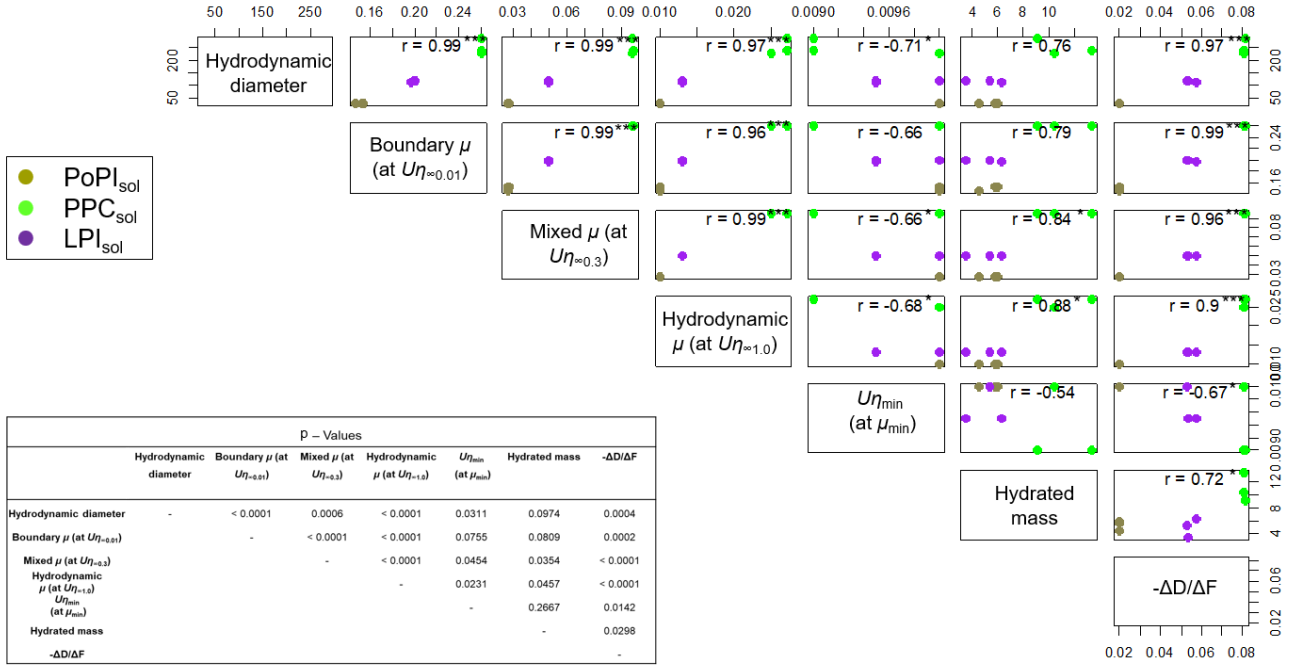

p – Values

	Hydrodynamic diameter	Boundary μ (at $U\eta_{\infty 0.01}$)	Mixed μ (at $U\eta_{\infty 0.3}$)	Hydrodynamic μ (at $U\eta_{\infty 1.0}$)	$U\eta_{min}$ (at μ_{min})	Hydrated mass	-ΔD/ΔF
Hydrodynamic diameter	-	< 0.0001	0.0006	< 0.0001	0.0311	0.0974	0.0004
Boundary μ (at $U\eta_{\infty 0.01}$)		-	< 0.0001	< 0.0001	0.0755	0.0809	0.0002
Mixed μ (at $U\eta_{\infty 0.3}$)			-	< 0.0001	0.0454	0.0354	< 0.0001
Hydrodynamic μ (at $U\eta_{\infty 1.0}$)				-	0.0231	0.0457	< 0.0001
$U\eta_{min}$ (at μ_{min})					-	0.2667	0.0142
Hydrated mass						-	0.0298
-ΔD/ΔF							-

Supplementary Figure S4. Pearson correlation (r) of instrumental data for 10 wt% protein solutions excluding WPI_{sol} and IPC_{sol}, where per protein data set n = 3. Spearman's rank was used to obtain *p-values* shown in the inset table and translated into *, **, *** indicating 0.05-0.001 in order of significance.

References

Adal, E., Sadeghpour, A., Connell, S., Rappolt, M., Ibanoglu, E., & Sarkar, A. (2017). Heteroprotein complex formation of bovine lactoferrin and pea protein isolate: A multiscale structural analysis. *Biomacromolecules, 18*(2), 625-635.

Akyol, H., Riciputi, Y., Capanoglu, E., Caboni, M. F., & Verardo, V. (2016). Phenolic Compounds in the Potato and Its Byproducts: An Overview. *International journal of molecular sciences, 17*(6), 835.

Andablo-Reyes, E., Yerani, D., Fu, M., Liamas, E., Connell, S., Torres, O., & Sarkar, A. (2019). Microgels as viscosity modifiers influence lubrication performance of continuum. *Soft Matter, 15*(47), 9614-9624.

Belloque, J., García, M., Torre, M., & Marina, M. (2002). Analysis of soyabean proteins in meat products: A review. *Critical Reviews in Food Science and Nutrition, 42*, 507-532.

Bouaouina, H., Desrumaux, A., Loisel, C., & Legrand, J. (2006). Functional properties of whey proteins as affected by dynamic high-pressure treatment. *International Dairy Journal, 16*(4), 275-284.

Bußler, S., Rumpold, B. A., Jander, E., Rawel, H. M., & Schlüter, O. K. (2016). Recovery and techno-functionality of flours and proteins from two edible insect species: Meal worm (Tenebrio molitor) and black soldier fly (Hermetia illucens) larvae. *Heliyon, 2*(12), e00218-e00218.

Chao, D., Jung, S., & Aluko, R. E. (2018). Physicochemical and functional properties of high pressure-treated isolated pea protein. *Innovative Food Science & Emerging Technologies, 45*, 179-185.

Chen, J., & Stokes, J. R. (2012). Rheology and tribology: Two distinctive regimes of food texture sensation. *Trends in Food Science & Technology, 25*(1), 4-12.

Chihi, M.-L., Mession, J.-l., Sok, N., & Saurel, R. (2016). Heat-Induced Soluble Protein Aggregates from Mixed Pea Globulins and β-Lactoglobulin. *Journal of Agricultural and Food Chemistry, 64*(13), 2780-2791.

Chojnicka, A., de Jong, S., de Kruif, C. G., & Visschers, R. W. (2008). Lubrication Properties of Protein Aggregate Dispersions in a Soft Contact. *Journal of Agricultural and Food Chemistry, 56*(4), 1274-1282.

Dabija, A., Codina, G., Anca, G., Sanduleac, E., & Lacramioara, R. (2018). Effects of some vegetable proteins addition on yogurt quality. *Scientific Study and Research: Chemistry and Chemical Engineering, Biotechnology, Food Industry, 19*, 181-192.

Damodaran, S., & Arora, A. (2013). Off-Flavor Precursors in Soy Protein Isolate and Novel Strategies for their Removal. *Annual Review of Food Science and Technology, 4*(1), 327-346.

Edwards, P. J. B., & Jameson, G. B. (2014). Chapter 7 - Structure and Stability of Whey Proteins. In H. Singh, M. Boland & A. Thompson (Eds.), *Milk Proteins (Second Edition)* (pp. 201-242). San Diego: Academic Press.

Glumac, M., Ritzoulis, C., & Chen, J. (2019). Surface properties of adsorbed salivary components at a solid hydrophobic surface using a quartz crystal microbalance with dissipation (QCM–D). *Food Hydrocolloids, 97*, 105195.

Graf, B., Protte, K., Weiss, J., & Hinrichs, J. (2020). Concentrated whey as protein source for thermally stabilized whey protein-pectin complexes. *Journal of Food Engineering, 269*, 109760.

Guimarães, D., & Gasparetto, C. (2005). Whey proteins solubility as function of temperature and pH. *LWT - Food Science and Technology, 38*, 77-80.

Guzmán-González, M., Morais, F., Ramos, M., & Amigo, L. (1999). Influence of skimmed milk concentrate replacement by dry dairy products in a low fat set-type yoghurt model system. I: Use of whey protein concentrates, milk protein concentrates and skimmed milk powder. *Journal of the Science of Food and Agriculture, 79*(8), 1117-1122.

Hulmi, J. J., Lockwood, C. M., & Stout, J. R. (2010). Effect of protein/essential amino acids and resistance training on skeletal muscle hypertrophy: A case for whey protein. *Nutrition & Metabolism, 7*(1), 51.

Jayasena, V., Chih, H., & Abbas, S. (2011). Efficient isolation of lupin protein. *Food Australia, 63*, 306-309.
Kew, B., Holmes, M., Stieger, M., & Sarkar, A. (2020). Review on fat replacement using protein-based microparticulated powders or microgels: A textural perspective. *Trends in Food Science & Technology*.
Kilara, A., & Vaghela, M. N. (2004). 4 - Whey proteins. In R. Y. Yada (Ed.), *Proteins in Food Processing* (pp. 72-99): Woodhead Publishing.
Kokini, J. L., Kadane, J. B., & Cussler, E. L. (1977). Liquid texture perceived in the mouth. *Journal of Texture Studies, 8*(2), 195-218.
Lacroix, I. M. E., Dávalos Terán, I., Fogliano, V., & Wichers, H. J. (2019). Investigation into the potential of commercially available lesser mealworm (A. diaperinus) protein to serve as sources of peptides with DPP-IV inhibitory activity. *54*(3), 696-704.
Laiho, S., Williams, R. P. W., Poelman, A., Appelqvist, I., & Logan, A. (2017). Effect of whey protein phase volume on the tribology, rheology and sensory properties of fat-free stirred yoghurts. *Food Hydrocolloids, 67*, 166-177.
Lam, A. C. Y., Can Karaca, A., Tyler, R. T., & Nickerson, M. T. (2018). Pea protein isolates: Structure, extraction, and functionality. *Food Reviews International, 34*(2), 126-147.
Lesme, H., Rannou, C., Loisel, C., Famelart, M.-H., Bouhallab, S., & Prost, C. (2019). Controlled whey protein aggregates to modulate the texture of fat-free set-type yoghurts. *International Dairy Journal, 92*, 28-36.
Liu, K., Stieger, M., van der Linden, E., & van de Velde, F. (2016a). Effect of microparticulated whey protein on sensory properties of liquid and semi-solid model foods. *Food Hydrocolloids, 60*, 186-198.
Liu, K., Tian, Y., Stieger, M., van der Linden, E., & van de Velde, F. (2016b). Evidence for ball-bearing mechanism of microparticulated whey protein as fat replacer in liquid and semi-solid multi-component model foods. *Food Hydrocolloids, 52*, 403-414.
Liu, R., Wang, L., Liu, Y., Wu, T., & Zhang, M. (2018). Fabricating soy protein hydrolysate/xanthan gum as fat replacer in ice cream by combined enzymatic and heat-shearing treatment. *Food Hydrocolloids, 81*, 39-47.
Nadal, P., Canela, N., Katakis, I., & O'Sullivan, C. K. (2011). Extraction, Isolation, and Characterization of Globulin Proteins from Lupinus albus. *Journal of Agricultural and Food Chemistry, 59*(6), 2752-2758.
Nastaj, M., Terpiłowski, K., & Sołowiej, B. G. (2020). The effect of native and polymerised whey protein isolate addition on surface and microstructural properties of processed cheeses and their meltability determined by Turbiscan. *International Journal of Food Science & Technology, 55*(5), 2179-2187.
Nishanthi, M., Chandrapala, J., & Vasiljevic, T. (2017). Compositional and structural properties of whey proteins of sweet, acid and salty whey concentrates and their respective spray dried powders. *International Dairy Journal, 74*, 49-56.
Oliete, B., Yassine, S. A., Cases, E., & Saurel, R. (2019). Drying method determines the structure and the solubility of microfluidized pea globulin aggregates. *Food Research International, 119*, 444-454.
Oliete Bonastre, P. F., Cases Eliane,Saurel Rémi. (2018). Modulation of the emulsifying properties of pea globulin soluble aggregates by dynamic high-pressure fluidization. *Innovative Food Science & Emerging Technologies, 47*, 292-300.
Pradal, C., & Stokes, J. R. (2016). Oral tribology: bridging the gap between physical measurements and sensory experience. *Current Opinion in Food Science, 9*, 34-41.
Prakash, S., Tan, D. D. Y., & Chen, J. (2013). Applications of tribology in studying food oral processing and texture perception. *Food Research International, 54*(2), 1627-1635.
Ralet, M.-C., & Guéguen, J. (2000). Fractionation of Potato Proteins: Solubility, Thermal Coagulation and Emulsifying Properties. *LWT - Food Science and Technology, 33*(5), 380-387.
Sánchez-Obando, J.-D., Cabrera-Trujillo, M. A., Olivares-Tenorio, M.-L., & Klotz, B. (2020). Use of optimized microparticulated whey protein in the process of reduced-fat spread and petit-suisse cheeses. *LWT, 120*, 108933.

Sarkar, A., Andablo-Reyes, E., Bryant, M., Dowson, D., & Neville, A. (2019). Lubrication of soft oral surfaces. *Current Opinion in Colloid & Interface Science, 39*, 61-75.

Sarkar, A., & Dickinson, E. (2020). Sustainable food-grade Pickering emulsions stabilized by plant-based particles. *Current Opinion in Colloid & Interface Science*.

Sarkar, A., Kanti, F., Gulotta, A., Murray, B. S., & Zhang, S. (2017). Aqueous lubrication, structure and rheological properties of whey protein microgel particles. *Langmuir, 33*(51), 14699-14708.

Sarkar, A., & Krop, E. M. (2019). Marrying oral tribology to sensory perception: a systematic review. *Current Opinion in Food Science, 27*, 64-73.

Sats, A., Mootse, H., Pajumägi, S., Pisponen, A., Tatar, V., & Poikalainen, V. (2014). Estimation of Particle Size Distribution in Bovine Colostrum Whey by Dynamic Light Scattering (DLS) Method. *Agronomy Research, 12*.

Schmidt, J. M., Damgaard, H., Greve-Poulsen, M., Sunds, A. V., Larsen, L. B., & Hammershøj, M. (2019). Gel properties of potato protein and the isolated fractions of patatins and protease inhibitors – Impact of drying method, protein concentration, pH and ionic strength. *Food Hydrocolloids, 96*, 246-258.

Sousa, I. M. N., Morgan, P. J., Mitchell, J. R., Harding, S. E., & Hill, S. E. (1996). Hydrodynamic Characterization of Lupin Proteins: Solubility, Intrinsic Viscosity, and Molar Mass. *Journal of Agricultural and Food Chemistry, 44*(10), 3018-3021.

Stokes, J. R., Boehm, M. W., & Baier, S. K. (2013). Oral processing, texture and mouthfeel: From rheology to tribology and beyond. *Current Opinion in Colloid & Interface Science, 18*(4), 349-359.

Stokes, J. R., Macakova, L., Chojnicka-Paszun, A., de Kruif, C. G., & de Jongh, H. H. J. (2011). Lubrication, Adsorption, and Rheology of Aqueous Polysaccharide Solutions. *Langmuir, 27*(7), 3474-3484.

Veldhorst, M., Smeets, A., Soenen, S., Hochstenbach-Waelen, A., Hursel, R., Diepvens, K., Lejeune, M., Luscombe-Marsh, N., & Westerterp-Plantenga, M. (2008). Protein-induced satiety: Effects and mechanisms of different proteins. *Physiology & Behavior, 94*(2), 300-307.

Voigt, W. U. (1889). The relationship between the two elasticity constants isotropic body. *Wiedmann's annalen der phys chem, 38*, 573-587.

Waglay, A., Achouri, A., Karboune, S., Zareifard, M. R., & L'Hocine, L. (2019). Pilot plant extraction of potato proteins and their structural and functional properties. *LWT, 113*, 108275.

Wang, S., Errington, S., & Yap, H. (2008). Studies on carotenoids from lupin seeds. In (pp. 198-202). Canterbury: International Lupin Association.

Xu, F., Liamas, E., Bryant, M., Adedeji, A. F., Andablo-Reyes, E., Castronovo, M., Ettelaie, R., Charpentier, T. V. J., & Sarkar, A. (2020a). A Self-Assembled Binary Protein Model Explains High-Performance Salivary Lubrication from Macro to Nanoscale. *7*(1), 1901549.

Xu, F., Liamas, E., Bryant, M., Adedeji, A. F., Andablo-Reyes, E., Castronovo, M., Ettelaie, R., Charpentier, T. V. J., & Sarkar, A. (2020b). A Self-Assembled Binary Protein Model Explains High-Performance Salivary Lubrication from Macro to Nanoscale. *Advanced Materials Interfaces, 7*(1), 1901549.

Yi, L., Lakemond, C. M. M., Sagis, L. M. C., Eisner-Schadler, V., van Huis, A., & van Boekel, M. A. J. S. (2013). Extraction and characterisation of protein fractions from five insect species. *Food Chemistry, 141*(4), 3341-3348.

Zembyla, M., Liamas, E., Andablo-Reyes, E., Gu, K., Krop, E. M., Kew, B., & Sarkar, A. (2021). Surface adsorption and lubrication properties of plant and dairy proteins: A comparative study. *Food Hydrocolloids, 111*, 106364.

Zhang, S., Holmes, M., Ettelaie, R., & Sarkar, A. (2020a). Pea protein microgel particles as Pickering stabilisers of oil-in-water emulsions: Responsiveness to pH and ionic strength. *Food Hydrocolloids, 102*, 105583.

Zhang, T., Guo, J., Chen, J.-F., Wang, J.-M., Wan, Z.-L., & Yang, X.-Q. (2020b). Heat stability and rheological properties of concentrated soy protein/egg white protein composite microparticle dispersions. *Food Hydrocolloids, 100*, 105449.

949

950